NUREG/CR-1800
BNL-NUREG-51298

WATER REACTOR SAFETY RESEARCH DIVISION

QUARTERLY PROGRESS REPORT
JULY 1 - SEPTEMBER 30, 1980

Date Published - November 1980

DEPARTMENT OF NUCLEAR ENERGY, BROOKHAVEN NATIONAL LABORATORY
UPTON, NEW YORK 11973

Prepared for the U.S. Nuclear Regulatory Commission
Office of Nuclear Regulatory Research
Contract No. DE-AC02-76CH00016

NUREG/CR-1800
BNL-NUREG-51298
AN R-1,4,5

NUREG/CR--1800
TI85 015884

WATER REACTOR SAFETY RESEARCH DIVISION

QUARTERLY PROGRESS REPORT
JULY 1 - SEPTEMBER 30, 1980

HERBERT J.C. KOUTS, Department Chairman
WALTER Y. KATO, Deputy Chairman

Principal Investigators:

N. Abuaf — M.M. Levine
R.J. Cerbone — P. Saha
D. van Rooyen

Compiled by: Anthony J. Romano

Manuscript Completed: October 1980

DEPARTMENT OF NUCLEAR ENERGY
BROOKHAVEN NATIONAL LABORATORY, ASSOCIATED UNIVERSITIES, INC.
UPTON, NEW YORK 11973

Prepared for the
REACTOR SAFETY RESEARCH DIVISION
OFFICE OF NUCLEAR REGULATORY RESEARCH
U.S. NUCLEAR REGULATORY COMMISSION
CONTRACT NO. DE-AC02-76CH00016
FIN Nos.:

A-3014 — A-3045
A-3208 — A-3215

EB

Available from
GPO Sales Program
Division of Technical Information and Document Control
U.S. Nuclear Regulatory Commission
Washington, D.C. 20555
and
National Technical Information Service
Springfield, Virginia 22161

FOREWORD

The Water Reactor Safety Research Programs Quarterly Report describes current activities and technical progress in the programs at Brookhaven National Laboratory sponsored by the USNRC Division of Reactor Safety Research. The projects reported each quarter are the following: LWR Thermal/Hydraulic Development, Advanced Code Evaluation, TRAC Code Assessment, and Stress Corrosion Cracking of PWR Steam Generator Tubing.

The previous reports, BNL-NUREG-50624, BNL-NUREG-50661, BNL-NUREG-50683, BNL-NUREG-50747, BNL-NUREG-50785, BNL-NUREG-50820, BNL-NUREG-50883, BNL-NUREG-50931, BN-NUREG-50978, BNL-NUREG-51015, BNL-NUREG-51081, BNL-NUREG-51131, BNL-NUREG-51178, BNL-NUREG-51218, and BNL-NUREG-51255 have covered the periods October 1, 1976 through June 30, 1980.

WATER REACTOR SAFETY RESEARCH

TABLE OF CONTENTS

I. LIGHT WATER REACTOR SAFETY

SUMMARY

A summary of all the experimental results for the Thermal/Hydraulic Development Program, i.e., pressure distributions, transverse distributions of the chordal averaged void fraction at given axial locations, and the area averaged void fraction distributions are presented. The effects of the flow parameters studied, i.e., inlet temperature, inlet mass flux and exit pressure on the recorded data are highlighted. A final draft report on the research was completed and submitted to NRC.

RAMONA-III is being tested and modified to calculate small pipe break LOCAs in a BWR. During this reporting period the following have been demonstrated: (1) ability to track water level in the downcomer; (2) ability to calculate reverse flow except in the riser; (3) ability to calculate two-phase flow outside the core; (4) ability to model cold water injection into two-phase fluid above the core; and (5) capability to run in a reasonable amount of time. More work is needed to adequately determine level in the core-riser region. The code was also modified to calculate a transient with power versus time as input. RAMONA-III is being applied to the "Half-ATWS" and rod drop accidents to give technical assistance to regulatory personnel.

The MARK II once-through steam generator model has been implemented in the IRT code and is currently being tested for an over cooling transient for a typical B&W plant. The results are being compared with similar results obtained using the MARK I model. The loop momentum equation, with a main coolant pump model, has been incorporated into a separate version of IRT and tested. The new model is currently being incorporated into the main version of the code.

The version of the RETRAN code at BNL has been modified to improve the plotting capability on the BNL computer.

Work on the independent assessment of TRAC-P1A has been terminated during the reporting quarter since an up-to-date version of TRAC i.e., TRAC-PD2, was received at BNL in July 1980. However, for the sake of completeness, a few simulations of the Super-CANON, RPI phase-separation, and FRIGG rod bundle tests have been performed with TRAC-P1A. The most notable of these simulations is the one-dimensional steady-state calculation obtained for a FRIGG rod bundle test. A converged solution was finally achieved with the two-fluid model of TRAC-P1A after the code was slightly modified at BNL. Specifically, the relative velocity used for the vapor generation calculations was changed from the current value to a time-averaged value. The results of these calculations, as well as others obtained by using TRAC-P1A at BNL, are being documented in three topical reports.

The TRAC-PD2, Version 25.3, has been made operational on the BNL computer. Seven of the LASL-supplied sample problems have been run successfully. However, the running times at BNL are somewhat longer than those at LASL. Efforts are underway to reduce the running time as much as possible. At the request of USNRC, a task involving the preparation of a final report on the

International Standard Problem 8 calculations was undertaken during this quarter. More than 50 percent of the task has been completed, and the report should be available in the next quarter.

1. Light Water Reactor Thermal/Hydraulic Development Program

1.1 Flashing Experiments (N. Abuaf)

A summary of the results, i.e., pressure distributions and area averaged void profiles, will be presented; the effects of the flow parameters, namely, flow rate, inlet temperature and exit pressure will be highlighted.

1.1.1 149 C Inlet Temperature Runs

Figure 1.1 depicts the axial distributions of the pressure (A) and the area averaged void fraction (B) for six experiments performed at 149 C inlet temperature and several inlet mass fluxes. A typical run (like Runs 291-295) consisted of two pressure drop measurements (Runs 291 and 295) and two consecutive transverse chordal averaged void fraction measurements (Runs 292 and 293) which were used in the calculation of the area averaged void fraction at a given axial location. The data presented in Figure 1.1 and the following figures are the average values of the pressure and area averaged void fractions calculated from the specific experiments. Runs 264-266 (open circles) were performed at an inlet temperature of 149 C, and an inlet mass flux of 2860 kg/m^2s. The inlet pressure for these runs is 515.2 kPa, corresponding to a high degree of subcooling; since the loop system is solid without a steam bubble in the condensing tank, single phase flow exists through the whole test section. The pressure distribution (Figure 1.1a) shows a decrease due to accelerational effects in the converging section and a typical single-phase pressure recovery in the diverging section. The area averaged void profiles plotted in Figure 1.1b depict an all liquid situation everywhere along the test section. Increasing the inlet mass flux to 3170 kg/m^2s, (Runs 291-295, open square), for the inlet temperature of 148.9 C, and pulling a steam bubble in the condensing tank increases the pressure drop in the converging section, bringing the experimental conditions close to the onset of flashing. The pressure once again decreases in the converging section, drops below the saturation pressure $P_s(T_{in})$, at the inlet temperature, reaches an undershoot of almost 60 kPa at the throat and levels off in the diverging section after an initial pressure recovery near pressure Taps 25-27. An additional pressure recovery is once again observed in the diverging section of the nozzle starting at pressure Tap 35. The area averaged void distributions plotted for the same experiment (Runs 291-295) show a single phase all-liquid condition in the converging section, with void formation starting at Tap 26. The void fraction then increases reaching a maximum value of about 0.25 and then decreases; these results are typically the same as those obtained with the low activity single beam densitometer under recondensation conditions. Increasing the inlet mass flux further to 3580 kg/m^2s (Runs 284-288) for an inlet temperature of 149.2 C, causes the inlet pressure to increase, in addition, the accelerational pressure drops in the converging section. Under flashing conditions with a steam bubble in the condensing tank, the inlet pressure in the BNL loop cannot be controlled independently of the flow rate. The variation of the inlet pressure with mass flow rate and condensing tank pressure is determined mainly by the pump and loop characteristics. The pressure distribution for Runs 284-288 show a smaller recovery than the previous experiment (Runs 291-295). The area averaged void profiles for Runs 284-288 depict a single phase all liquid condition in the converging section, the voids begin to be

generated between pressure Taps 25 (Throat) and 26. The slight pressure recovery observed in the diverging section is reflected by the constancy of the area averaged void fraction downstream of Tap 33. Upon further increasing the inlet mass fluxes to 4290 kg/m^{2}s, 5740 kg/m^{2}s, 6450 kg/m^{2}s, Runs 273-277, Runs 278-283, Runs 296-301 respectively, the test section inlet pressures are increased to 572.8 kPa, 688.2 kPa and 765.8 kPa respectively. The area averaged void fractions for all the latter runs show a single phase-all liquid in the converging section. Flashing inception seems to occur between Taps 25 and 26, and the area averaged void fraction increases monotonically to the exit of the nozzle. The area averaged voids at the exit reach a value of 0.65 and remains constant for an increase of inlet mass flux from 5742 kg/m^{2}s (Runs 278-283) to 6450 kg/m^{2}s (Runs 296-301). One interesting observation which is common to all of the remaining data presented with subcooled inlet conditions is that for a constant inlet temperature, independent of the mass flow rate and inlet subcooling, flashing inception always occurs very close to the throat and the pressure undershoot below saturation seems to be almost constant for all the experiments presented in Figure 1.1, $p_s(T_{in}) - p_{Tap} = 50 \pm 10$ kPa. For a 150 C inlet temperature, and for very low depressurization rates the extrapolated Alamgir-Lienhard correlation (1979) predicts an undershoot of 84.9 kPa. We note however, that the depressurization rates in the BNL experiments are much below the range for which the Alamgir Lienhard correlation was derived. Similarly the correlation proposed by Lackme (1979a, b) would have predicted an undershoot below the saturation pressure equal to 24 kPa.

In Figure 1.2 the axial distributions of pressure (A) and area averaged void fraction (B) are presented for 4 Runs performed at an inlet temperature of 149 C, a constant inlet mass flux of 4300 kg/m^{2}s and a decreasing nozzle exit or condensing tank pressure. The first experiments Runs 268-272, were performed at an inlet temperature of 149 C, an inlet pressure of 575.9 kPa and an inlet mass flux of 4300 kg/m^{2}s. The steam bubble in the condensing tank was comparatively small with conditions very close to saturation, T_{ct} = 149.1 C, and p_{ct} = 454.2 kPa. The pressure distribution is typical for a single phase variation down to the nozzle throat, rising a little between Taps 25 and 27 and then remaining almost constant in the diverging section of the venturi. The area averaged void fraction show flashing inception between pressure Taps 25 and 26 and a monotonic increase in the diverging section. Increasing the volume of the steam bubble in the condensing tank to twice its original value did not affect the results (Runs 273-277). During the third experiment presented (Runs 304-307), cold water was sprayed into the condensing tank thus decreasing its temperature and pressure, and also affecting the test section exit pressure. The test section inlet temperature was maintained at its original value of 149 C by the addition of more heat into the subcooled water flow upstream of the test section. For runs 304-307, the condensing tank temperature and pressure were 147.6 C and 439.9 kPa respectively compared to the original values of 148.8 C and 451.7 kPa during Runs 273-277. The effect of this variation has a negligible effect on the pressure distributions; the area averaged void fraction is observed to be only slightly higher for positions close to the exit of the nozzle. During the next series of Runs (Runs 309-311), spray cooling was still increased bringing the condensing tank pressure and temperatures to 378.3 kPa and 142.2 C respectively. This was accompanied by decreasing the test section inlet

pressure to 555.9 kPa, while maintaining the inlet temperature at 149.1 C and the inlet mass flux at 4330 kg/m^2s. Although the whole pressure distribution in the test section was observed to be lower than the previous ones, no drastic changes were observed in the area averaged void profiles (Figure 1.2a and b). In Figures 1.3 and 1.4 a three dimensional representation of the chordal averaged void fractions at various axial locations all along the test section are depicted for the last two experiments (Run 306 and Run 310). Although the area averaged void fraction values are the same for both runs, the transverse chordal averaged void fraction distributions are very different near and at the exit of the nozzle. Detailed transverse profiles of the chordal averaged void fractions for the two runs are also presented in Figures 1.5 and 1.6. In one case, (Run 306), the void distributions at Tap locations 47, 45, 43 and 41 are nonsymmetrical and more vapor is generated on the left hand side. For the void distributions presented in Figure 1.6 for Run 310 for the same axial locations, one observes that the profiles are symmetrical and a low void core is surrounded by an axially symmetrical high void region. The transverse distributions also affect the comparisons of the centerline diametrical averaged void fraction with the area averaged value at the same axial location. This fact is illustrated in Figures 1.2a and b, where the two void fractions are compared at the same axial location. For Run 306 (Figure 1.7a), the two values are close to each other and show the same dependance with axial distance. For Run 310 (Figure 1.7b), the diametrical averaged center line void fractions show a nearly linear increase with distance; the area averaged values, however, are higher at a given axial location downstream of the throat and show a different dependence with the axial distance. The error bars around the measured values represent the standard deviation calculated from the measurements performed at the same location.

These results clearly show the importance and effect of the transverse void fraction profiles on the area averaged or center line (diametrical averaged) values. Thus, in order to make valid comparisons between code predictions and experiments these effects must be carefully taken into account.

The condensing tank pressure could not be reduced further by increasing the cooling spray. Since the 520 kW heating was being fully used during these final runs to maintain the constant inlet temperature, additional heating capacity was unavailable.

1.1.2 121 C Inlet Temperature Runs

Runs similar to those described in Section 1.1.1 were also performed at a nominal test section inlet temperature of 121 C. Figure 1.8 depicts the axial distribution of pressure (A) and the area averaged void fraction (B) for five sets of experiments performed at an inlet temperature of 121 C and five mass fluxes. The first four experiments, Runs 141-144, Runs 145-148, Runs 133-136 and Runs 137-140 were performed with the five beam gamma densitometer while Runs 344-347 were performed with the high activity single beam gamma densitometer. Before describing the tests presented in Figure 1.8, it should be pointed out that the reproducibility of the results with the two systems of the gamma densitometer was also checked; the results are presented in Figure 1.9 which shows the axial pressure distributions as well as the area averaged

void fractions plotted as a function of the axial distance. Runs 133-136 were performed at an inlet mass flux of 4435 kg/m^{2}s and nozzle inlet pressure and temperature of 349 kPa and 121.2 C respectively. For this run, the transverse void profiles were measured with the five beam gamma densitometer system and are depicted as the open symbols in Figure 1.9a and b. Runs 322-325 were performed with the high activity single beam gamma densitometer at an inlet mass flux of 4410 kg/m^{2}s and nozzle inlet conditions, p_{in} = 342 kPa and T_{in} = 121 C. The results of these runs are presented in Figure 1.9 as the solid symbols. The repeatability of the results was excellent in the pressure distributions while the area averaged void fractions showed a wider scatter in the converging section than the five γ-beam system. Having satisfactorily checked the repeatability of the results with the two sets of measuring systems, one can now go back to Figure 1.8 and summarize the effect of increasing mass flux on the pressure and area averaged profiles. Runs 141-144 performed at an inlet mass flux of 2970 kg/m^{2}s, and nozzle inlet conditions of 241 kPa and 121.3 C, are once again typical of the single phase no flashing conditions. Increasing the inlet mass flux to 3700 kg/m^{2}s (Runs 145-148), 4435 kg/m^{2}s (Runs 133-136), 5900 kg/m^{2}s (Runs 137-140) and to 6640 kg/m^{2}s (Runs 344-347), increased the inlet pressure at the test section from 305 kPa to 538 kPa for a nominal constant inlet temperature of 121 C Similar observations as reported in the last section are clearly seen in Figure 1.8. The flashing inception once again occurs very close to the throat although the average void fraction data show a much wider scatter in the converging section of the nozzle and especially close to the throat. The pressure undershoots for all the flashing experiments presented in Figure 1.8 give a value of $p_s(T_{in}) - p_{Tap\ 25} = 40 \pm 19$ kPa. The constant value of the pressure distribution in the diverging section of the nozzle seems also to be the same for all the runs for the pressure scale presented in Figure 1.8a. The area averaged void profiles presented show a slight increase with increasing mass flux and remain therefore within a scatter of $\pm$ 0.05.

In Figure 1.10 the axial distribution of pressure (A) and area averaged void fraction (B) are presented for several runs performed at an inlet temperature of 121 C, a constant inlet mass flux of 4420 kg/m^{2}s and a decreasing nozzle exit or condensing tank pressure. All the runs presented in this figure were performed with the high activity single beam densitometer. After running a single phase-all liquid calibration run with detailed void distributions shown in Figure 1.11, Runs 339-342 were then performed at an inlet temperature of 121.2 C, an inlet pressure of 320 kPa and a mass flux of 4425 kg/m^{2}s. The condensing tank pressure was maintained at 240 kPa, causing a high back pressure at the exit of the nozzle, thereby creating a pressure recovery and a condensation zone in the diverging part of the test section. The detailed void fraction distributions for this run are depicted in Figure 1.12 as a function of axial distance.

Runs 322-326 were performed at very similar inlet conditions, G_{in} = 4410 kg/m^{2}s, p_{in} = 341 kPa, T_{in} = 121 C, except that the condensing tank pressure was reduced to 200 kPa. The resulting pressure distributions in the diverging section become constant and the area averaged void profile depicts a monotonic increase with the axial distance. The detailed void profiles for Runs 322-326 are presented in Figure 1.13, showing the regularly observed nonsymmetrical transverse void distributions. During the next experiment

(Runs 313-316), cold water was injected into the condensing tank, thus decreasing its temperature and pressure, and also affecting the test section exit pressure. For these runs (313-316) the test section inlet conditions were as follows: G_{in} = 4430 kg/m^{2}s, P_{in} = 341 kPa, T_{in} = 121 C, P_{ct} = 187 kPa and T_{ct} = 119 C. The detailed void profiles for these runs are presented in Figure 1.14. Upon further increasing the spray cooling the condensing tank conditions were decreased to P_{ct} = 157 kPa and T_{ct} = 113 C; the inlet pressure was reduced to 321 kPa, for the inlet temperature of 121 C and mass flux of 4430 kg/m^{2}s. Although the area averaged void fraction again do not appear to vary (see Figure 1.10b), the transverse chordal averaged void fraction distributions however, become symmetrical close to the exit of the nozzle. The detailed transverse void profiles for the latter runs (Run 320) are presented in Figure 1.15. The comments and observation reported in Section 1.1.1 when comparing the centerline diametrical averaged void with the area averaged value can be applied to these series of runs at a nominal inlet temperature of 121 C. The condensing tank temperature and pressure could not be reduced any further by increasing spray cooling; due to the given relatively high mass flow rate, the 520 kW heating capacity was already fully utilized.

During one of the experiments conducted at T_{in} = 121.3 C, P_{in} = 489 kPa and an inlet mass flux of 5890 kg/m^{2}s, a heater element failure resulted in a distribution of large amounts of MgO particulates throughout the water loop (Runs 149-153). Data recorded during this run is presented in Figure 1.16. The pressure distribution (Figure 1.16a) shows that the saturation pressure is reached at the nozzle throat and remains constant thereafter. In contrast to all other runs where a pressure undershoot was invariably observed at flashing inception, in Runs 149-153 in which particulates were present in the water, no pressure undershoot was observed. Thus flashing inception occurred practically under equilibrium conditions. The area averaged void profiles presented in Figure 1.16b once again depict a flashing inception at the throat and a monotonically increasing void fractions in the diverging section of the nozzle. Comparison of these results with those for Runs 137-140, performed under similar inlet conditions without the presence of particulates and where the pressure undershoot was observed at inception, does not show a drastic change in the observed pressure or void fraction profiles. (See Figure 1.8). Comparison of the detailed transverse void fraction distributions close to the nozzle exit (Taps 41, 43, 45 and 47) for Runs 137-140 with Runs 149-153, show that for the first series of Runs (137-140) the profiles at a given axial location are asymmetrical with a higher void region close to the left hand side wall while for the last series of Runs (149-153) the profiles at the same axial locations are symmetrical with respect to the tube centerline. This observation is similar to that previously reported in Section 1.1.1 when comparing Runs 304-307 with Runs 309-311 and in Section 1.1.2 when comparing Runs 318-321 with Runs 313-316.

1.1.3 100 C Inlet Temperature Runs

Experiments similar to those shown in Figures 1.1 and 1.8 were also performed at an inlet temperature of 100 C. Figure 1.17 depicts the axial distribution of the pressure (A) and the area averaged void fraction (B) for five

experiments performed at a constant inlet temperature and six increasing inlet mass fluxes. The five beam gamma densitometer was used for the void fraction profiles measured in all the runs presented in Figure 1.17. At the low mass flux runs (Runs 116-118), one observes an evaporation zone downstream of the throat followed by a pressure recovery and a condensation region. One point to be mentioned here is that at these low flow rates and close to the onset of flashing in the nozzle, the flow seemed to be quite unstable, specially for the 100 C inlet temperature runs. During these runs the flow configuration in the nozzle shifted from non-flashing to flashing and back again. Since our objective did not include the study of instabilities at flashing onset conditions, no detailed investigation of this observation was undertaken during the present work. The area averaged void fraction downstream of the nozzle throat is observed to increase with the inlet mass flux for a given axial location. Similar results were also obtained with the high activity single beam gamma densitometer and are presented in Figure 1.18. For all the results presented for an inlet temperature of 100 C, the flashing inception is observed to occur close to the nozzle throat, and the pressure undershoot below the saturation pressure at the obtained inlet temperature has a value of $p_s(T_{in}) - p_{Tap\ 25} = 14.7 \pm 16$ kPa.

1.1.4 Two-Phase Inlet Conditions

In addition to the subcooled inlet runs presented in Sections 1.1.1, 1.1.2 and 1.1.3, a series of runs were also performed with two phase inlet conditions. For all these runs the inlet temperature was kept at 121 C. The corresponding saturation pressure was 200 kPa. Figure 1.19 depicts the results obtained during these two-phase inlet runs. Run 368 was performed at an inlet mass flux of 1510 kg/m^{2}s and an inlet pressure 221 kPa, yielding a single phase flow through the whole test section. Runs 383-387 were performed at an inlet pressure which is very close to the saturation conditions and a pressure distribution and area averaged void profile which is very similar to the subcooled inlet conditions are observed. Runs 380-382 are made with a two phase very low void fraction inlet condition and a lower exit pressure, generating higher area averaged void fractions in the diverging section of the nozzle. A continuous decrease in the exit pressure, Runs 376-378 and Runs 373, 374, 3375, did not change the flow conditions (pressure and void fraction) in the converging section of the nozzle; the pressure distribution in the diverging section was affected with increases in the area averaged void fraction at the same axial locations. The detailed transverse chordal averaged void fraction distributions along the test section are presented in Figures 1.20 to 1.22. The distributions at an axial location close to the exit varies from a skewed profile (Run 386) in Figure 1.20, to a nonsymmetric one (Run 381, Figure 1.21), to a symmetrical high void distribution in Figure 1.22 for Run 377. Figure 1.23 represents similar results as those presented in Figure 1.19, clearly showing the transition from a single phase to a low void fraction entrance condition, when the inlet pressure and temperature are very close to saturation conditions. For the single phase inlet, the area averaged void starts increasing from Tap 27 (Figure 1.23b, Run 383-387). For a low void fraction inlet $\alpha_{in} = 0.05$, one observes a continuous decrease in the pressure in the venturi (Figure 1.23A, Run 370-372), while the area averaged void fractions seem to remain almost constant down to pressure Tap No. 23 from where it increases. The almost constant low void fraction in the converging

section of the test section is an interesting observation, since as the pressure is falling in the same locations, one would expect higher superheats (driving forces) for vapor generation and a fast increase in the vapor generation and void fractions. The effect of decreasing the mass flux from 1510 kgm/m^2s (Runs 373, 374, 3375) to 1065 kgm/m^2s (Runs 390-392) on the pressure distributions and area averaged profiles are depicted in Figure 1.24. The inlet temperature and pressure are on the saturation line and for the lower mass flux, the void fraction at the inlet is higher (~12%). The pressure distributions for the latter case are very similar for a continuous expansion in the nozzle and do not show the discontinuity at the throat as observed for Runs 373, 374, 3375. The area averaged void profile for Runs 390-392 shows a very slight increase in the converging section, reaching rapidly from pressure Tap ~21 onwards, reaching a value of almost 1.0 at the nozzle exit.

REFERENCES

ALAMGIR, Md., and LIENHARD, J. H., Personal communication (1979), "Correlation of Pressure Undershoot During Hot-Water Depressurization," J. of Heat Transfer, in press.

LACKME, C., "Propagation d'un Front de Vaporisation Dans un Tube Plein d'Eau Chaude Brusquement Detemdue," CEA-R-4986, (1979a).

LACKME, C., "Autovaporisation Dans une Conduite d'un Liquide Sature our Sour-Refroidi a l'Entree," CEA-R-4957, (1979b).

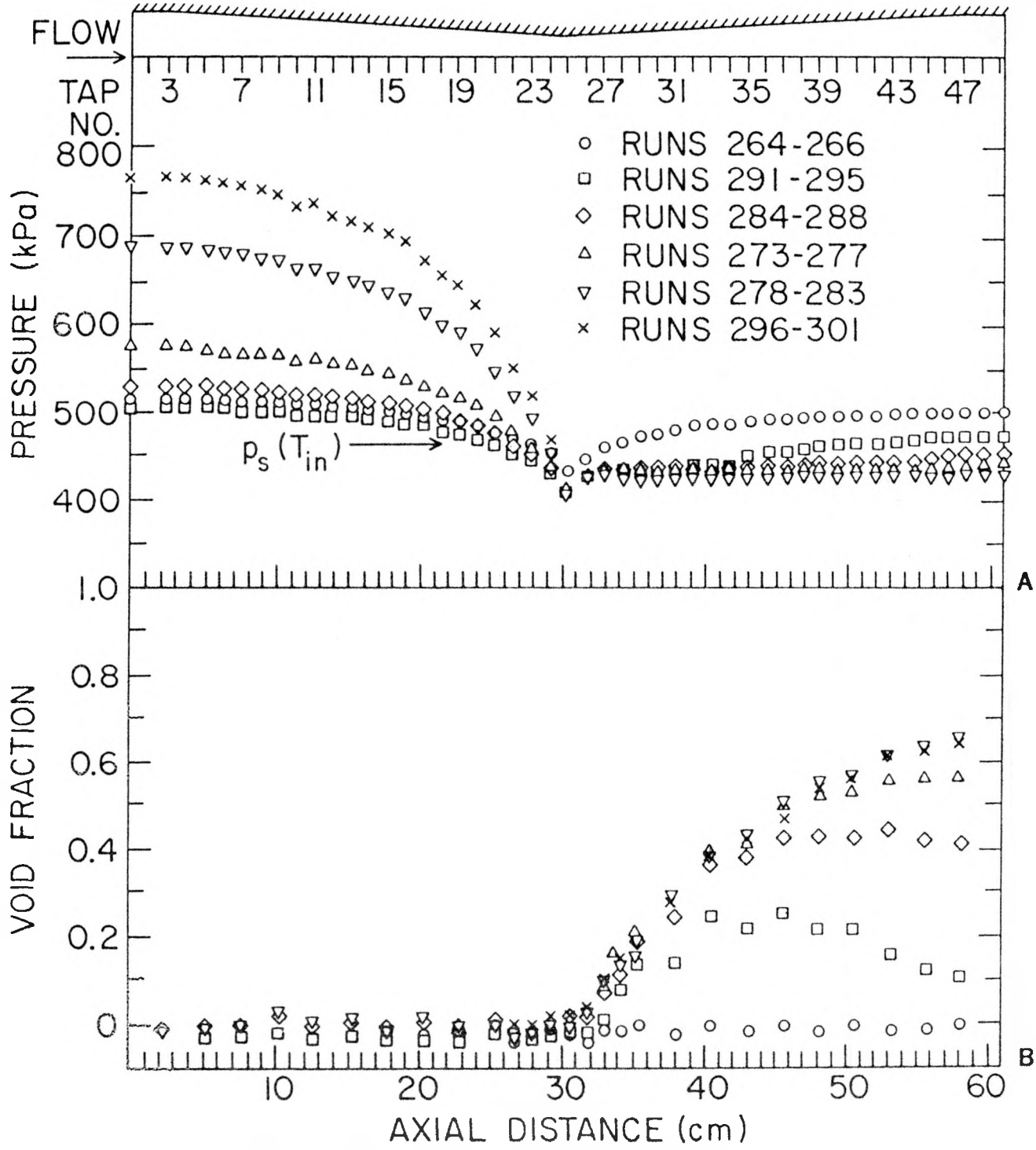

Figure 1.1 Axial Distributions of the Pressure (A) and Area Averaged Void Fraction (B) for Runs Performed at an Inlet Temperature of 149°C and Several Inlet Mass Fluxes (BNL Neg. No. 9-630-80).

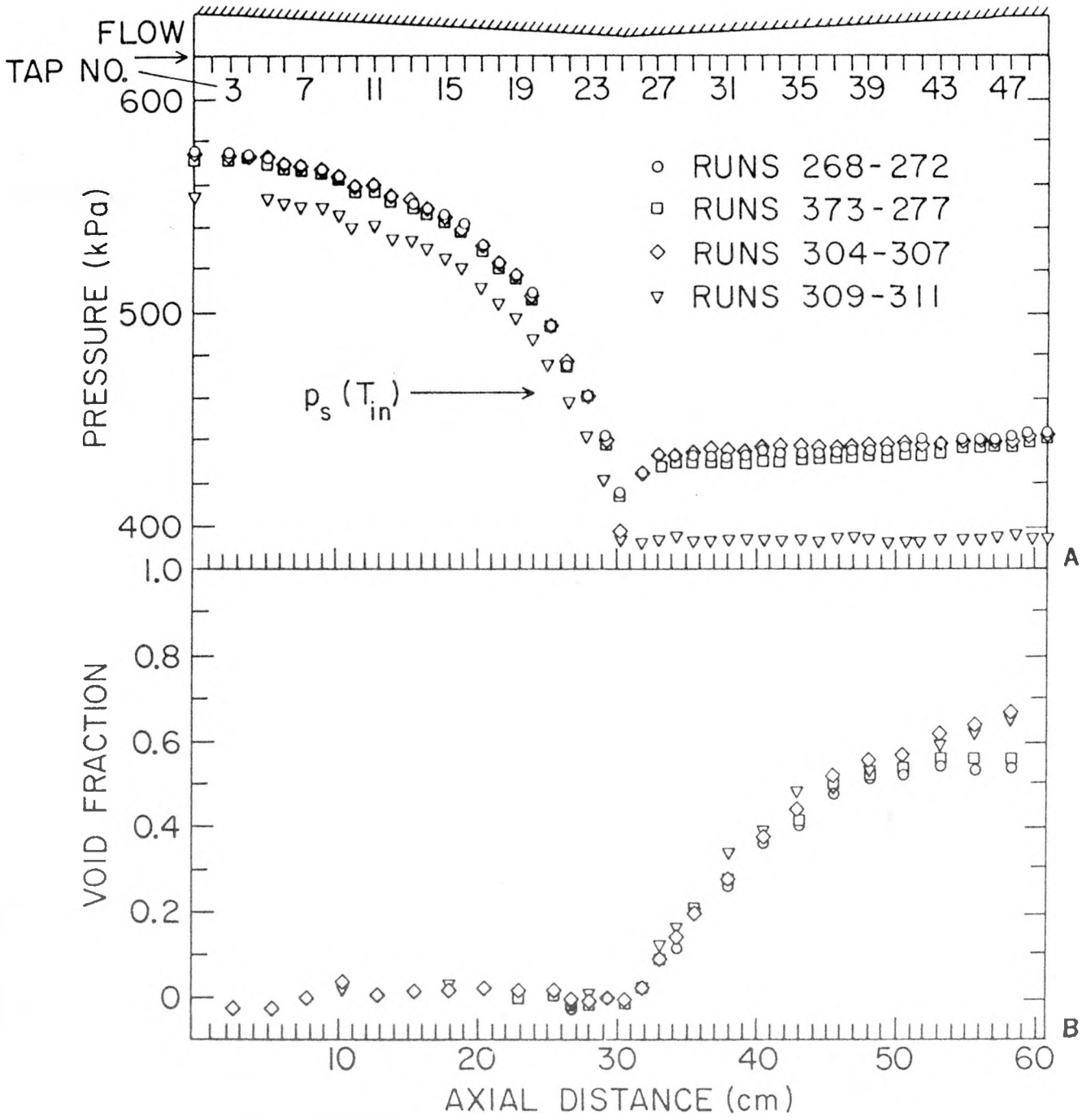

Figure 1.2 Axial Distributions of Pressure (A) and Area Averaged Void Fraction (B) for Runs Performed at an Inlet Temperature of 149°C, a Constant Inlet Mass Flux of 4300 kg/m^{2}s, and Decreasing Nozzle Exit or Condensing Tank Pressure (BNL Neg. No. 9-627-80).

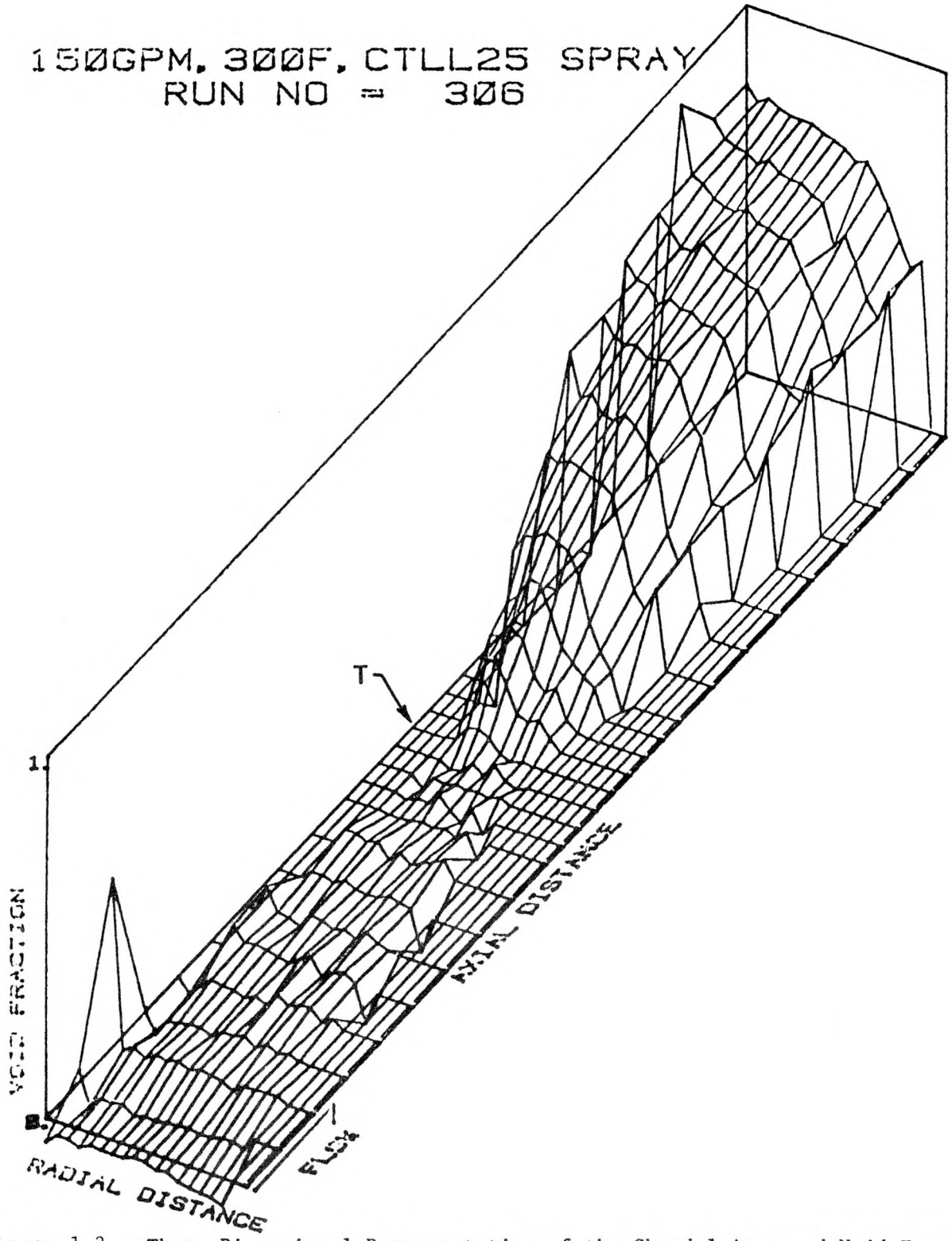

Figure 1.3 Three Dimensional Representation of the Chordal Averaged Void Fraction Distributions Along the Test Section (T Designates the Nozzle Throat) (BNL Neg. No. 9-601-80).

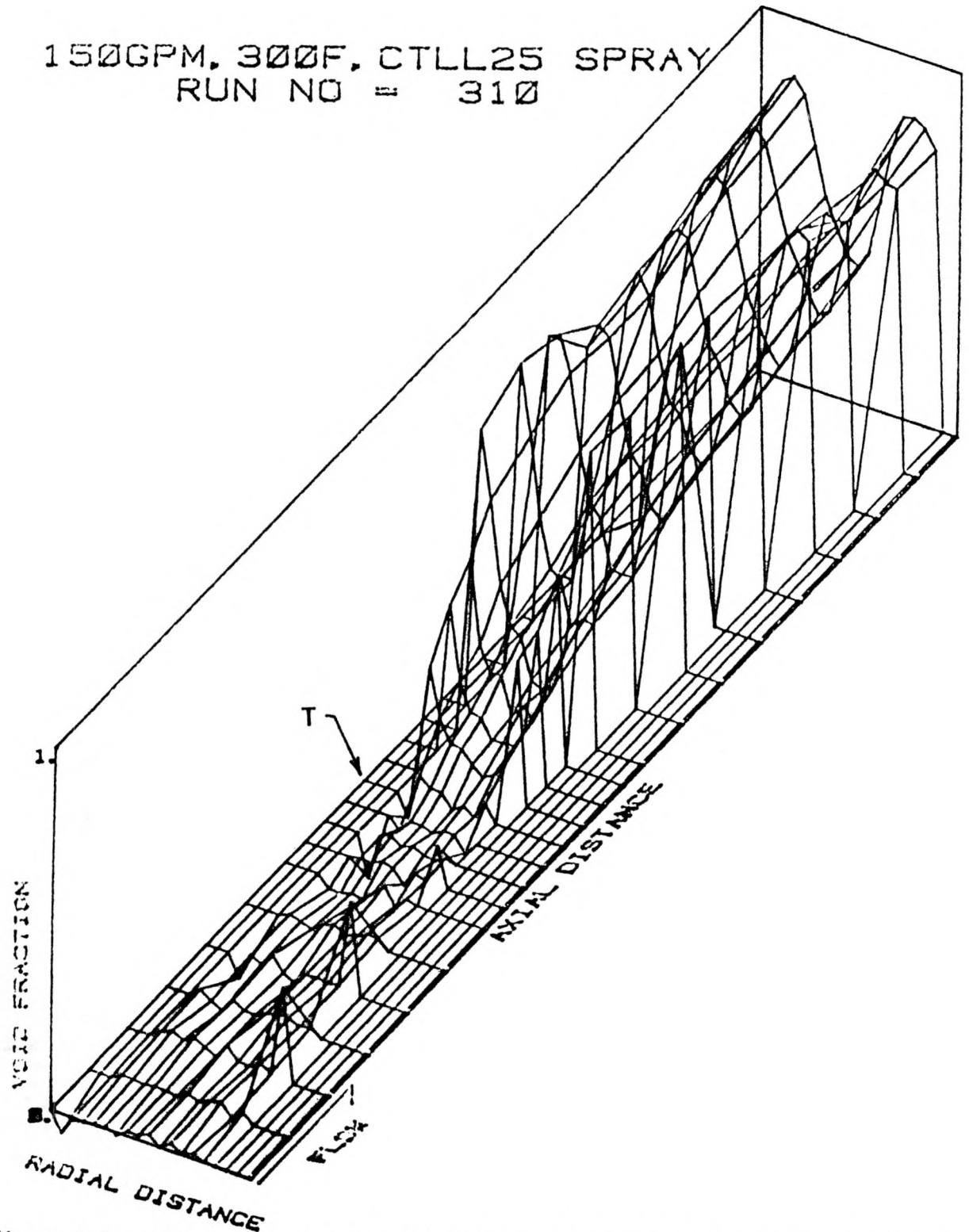

Figure 1.4 Three Dimensional Representation of the Chordal Averaged Void Fraction Distributions Along the Test Section (T Designates the Nozzle Throat) (BNL Neg. No. 9-599-80).

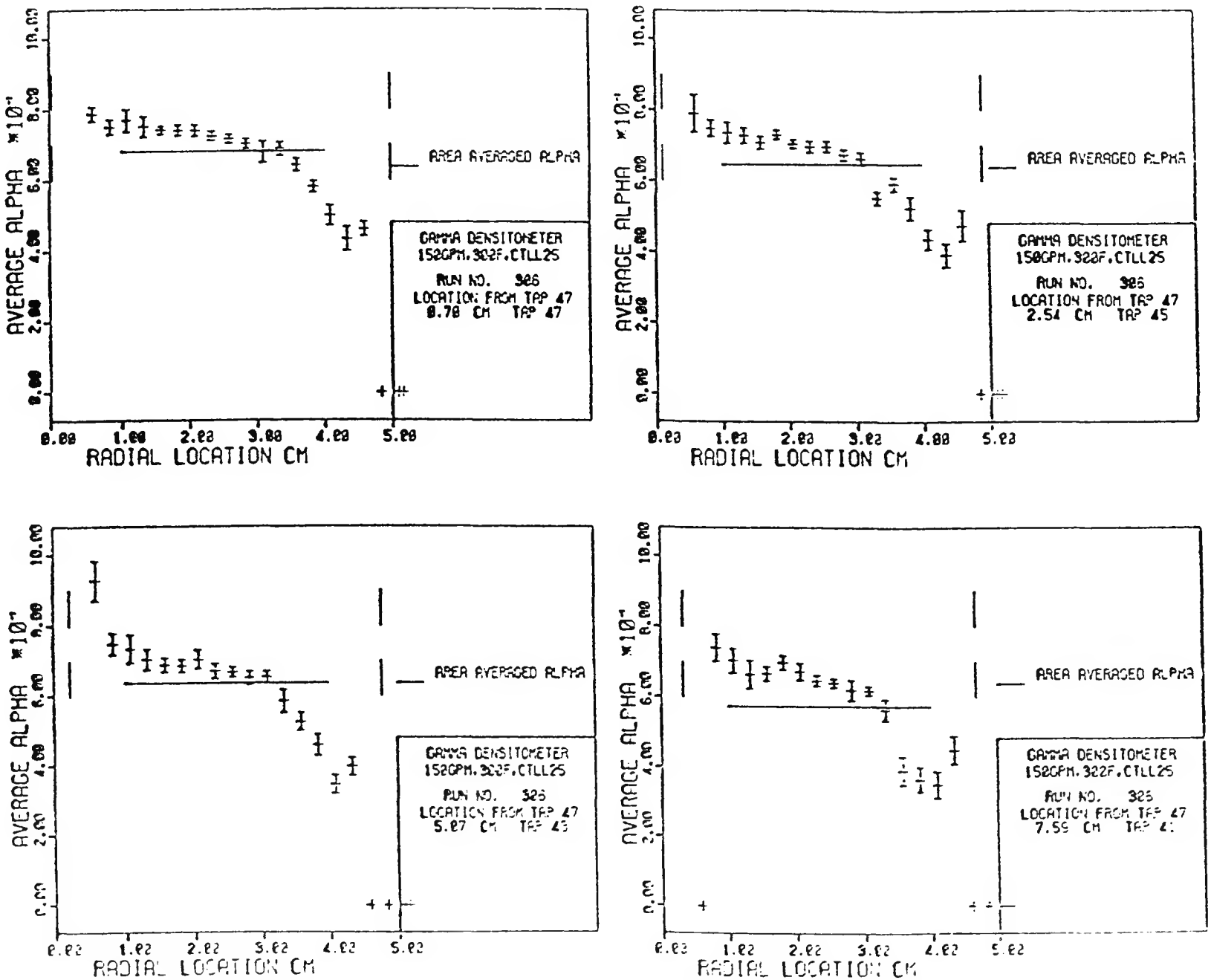

Figure 1.5 Radial Distributions of the Chordal Averaged Void Fractions at Four Axial Locations Obtained by the High Activity Single Beam Densitometer for Run 306 (BNL Neg. No. 9-603-80).

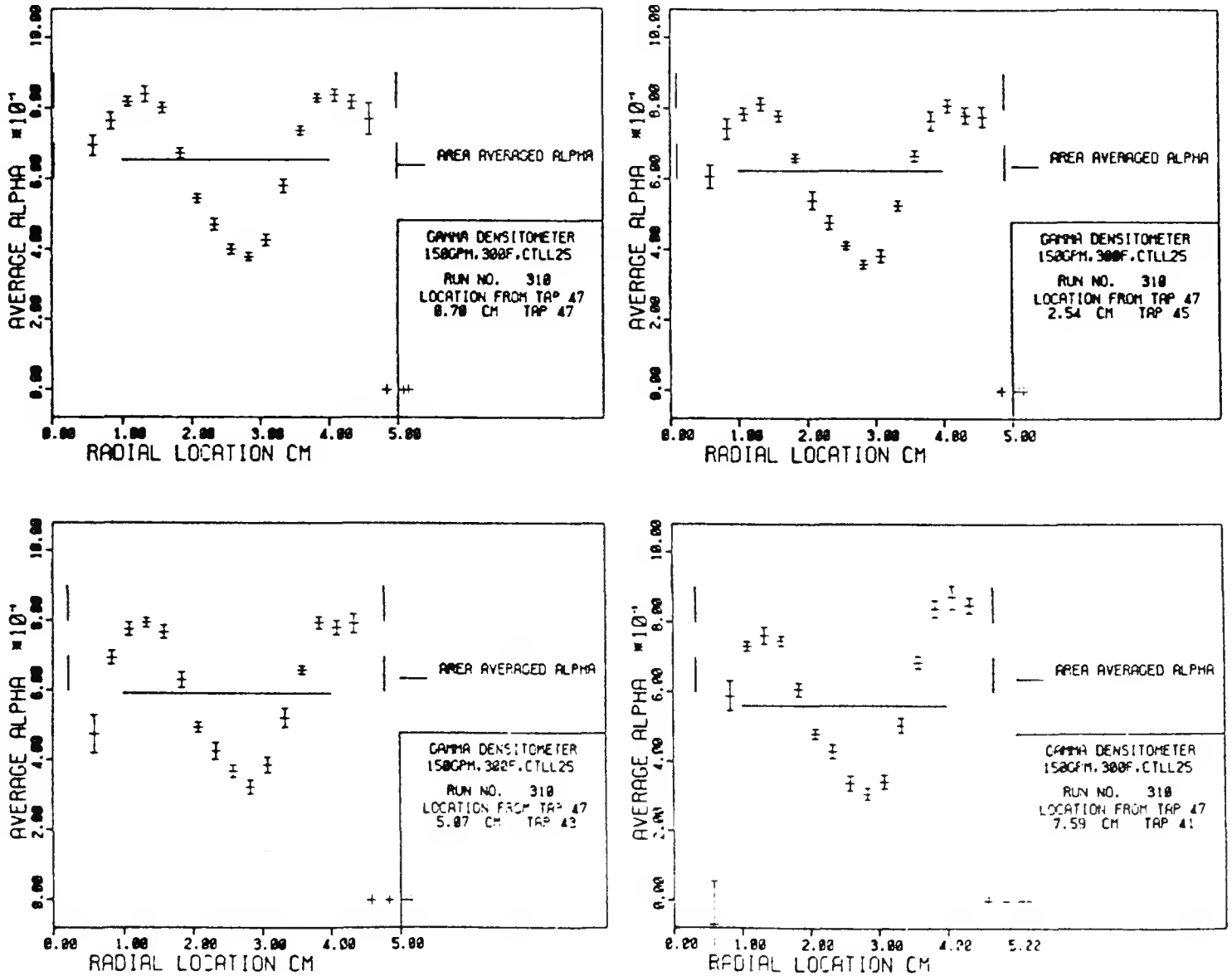

Figure 1.6 Radial Distributions of the Chordal Averaged Void Fractions at Four Axial Locations Obtained by the High Activity Angle Beam Densitometer for Run 310. (BNL Neg. No. 6-949-80)

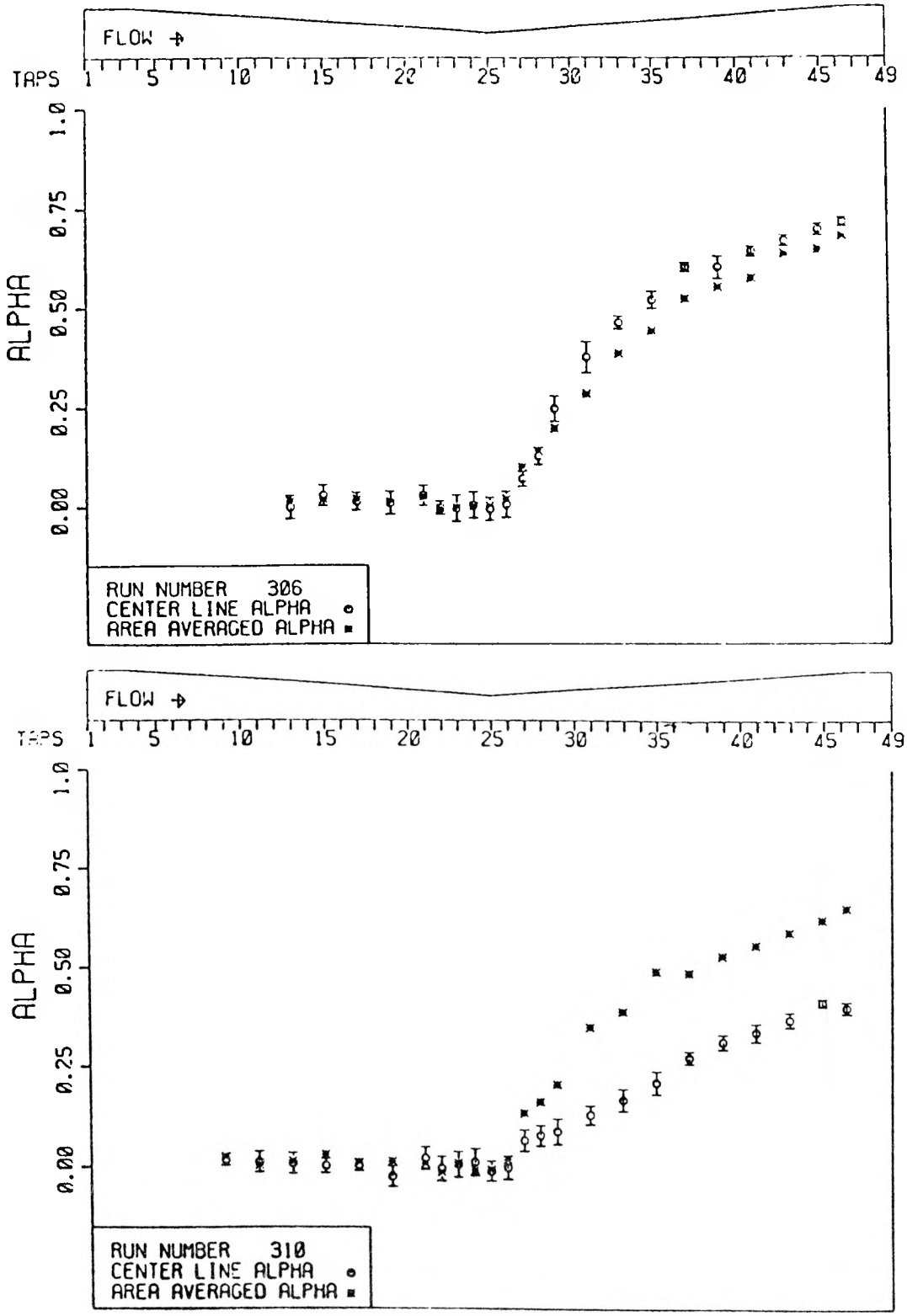

Figure 1.7 Comparison of Centerline Diametrical Averaged Void Fraction Distributions with the Area Averaged Void Fractions at the Same Axial Locations for Runs 306 and 310 (BNL Neg. No. 9-818-80).

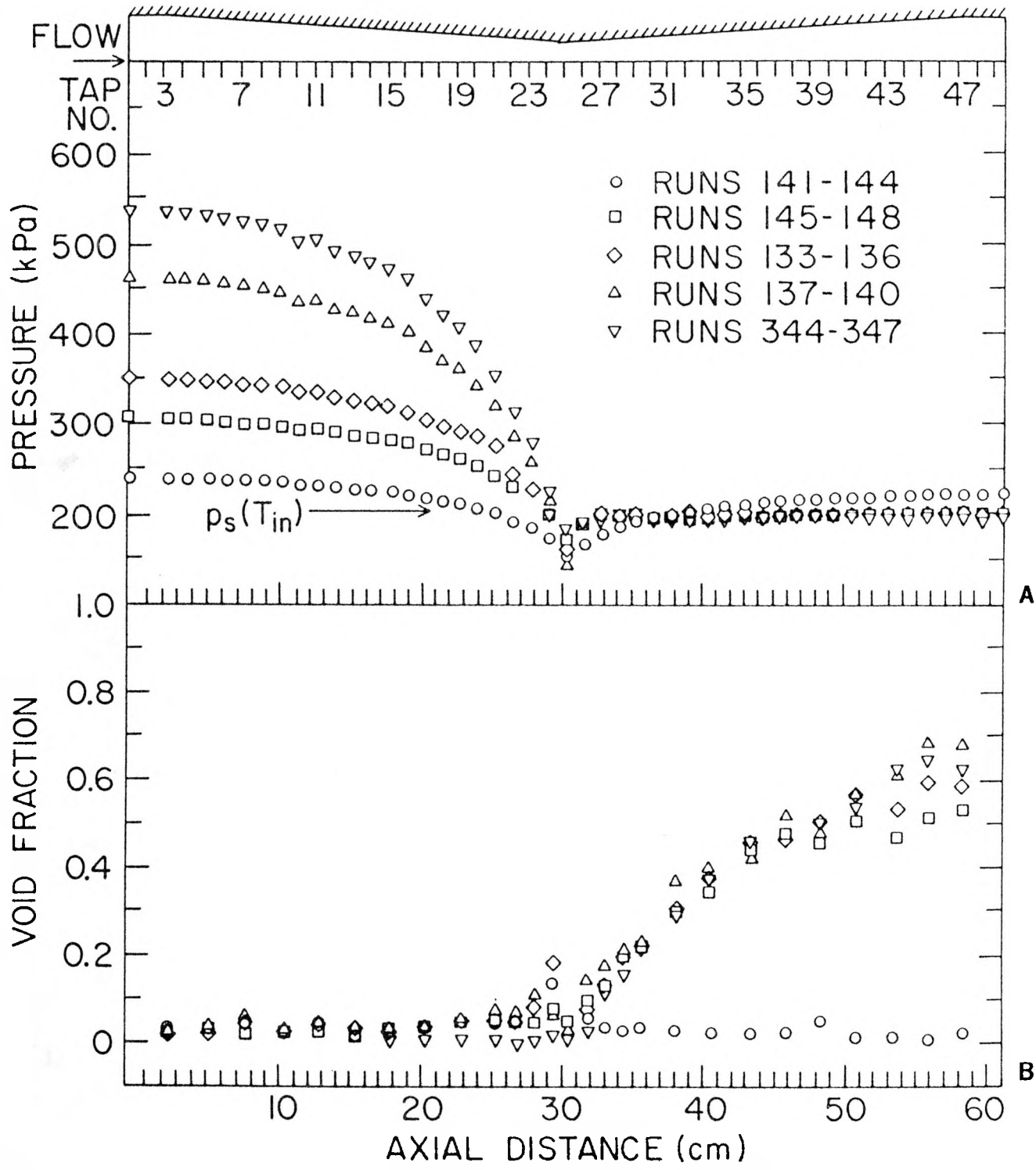

Figure 1.8 Axial Distributions of Pressure (A) and Area Averaged Void Fraction (B) for Five Runs Performed at an Inlet Temperature of 121°C and Increasing Inlet Mass Flux (BNL Neg. No. 9-624-80).

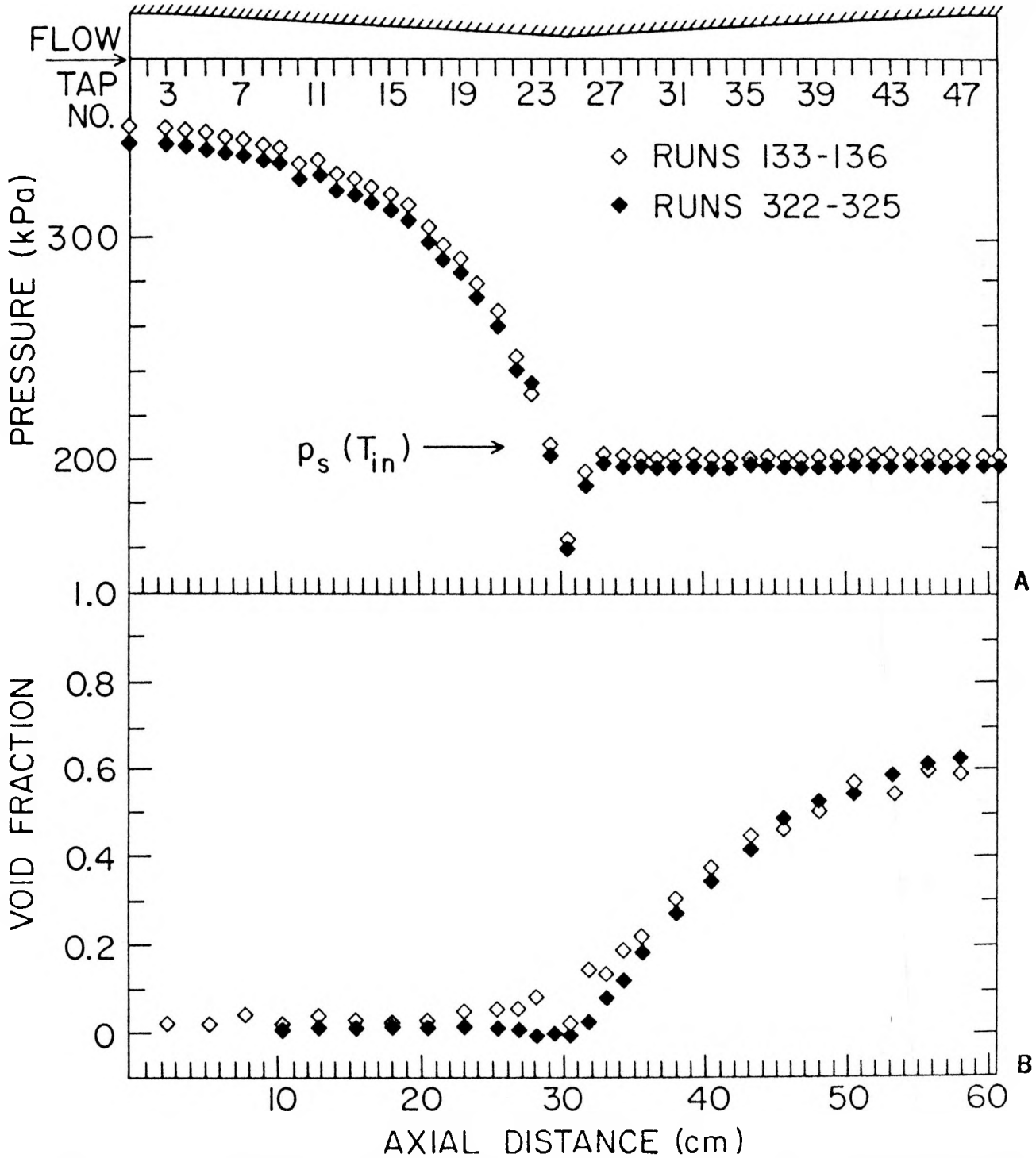

Figure 1.9 Comparison of Axial Distributions of Pressure (A) and Area Averaged Void Fraction (B) for Two Runs Performed Under "Identical" Conditions. Data in Runs 133-136 Were Recorded with the Five Beam Gamma Densitometer, While Data in Runs 322-325 Were Recorded with the High Activity Single Beam Densitometer (BNL Neg. No.9-629-80).

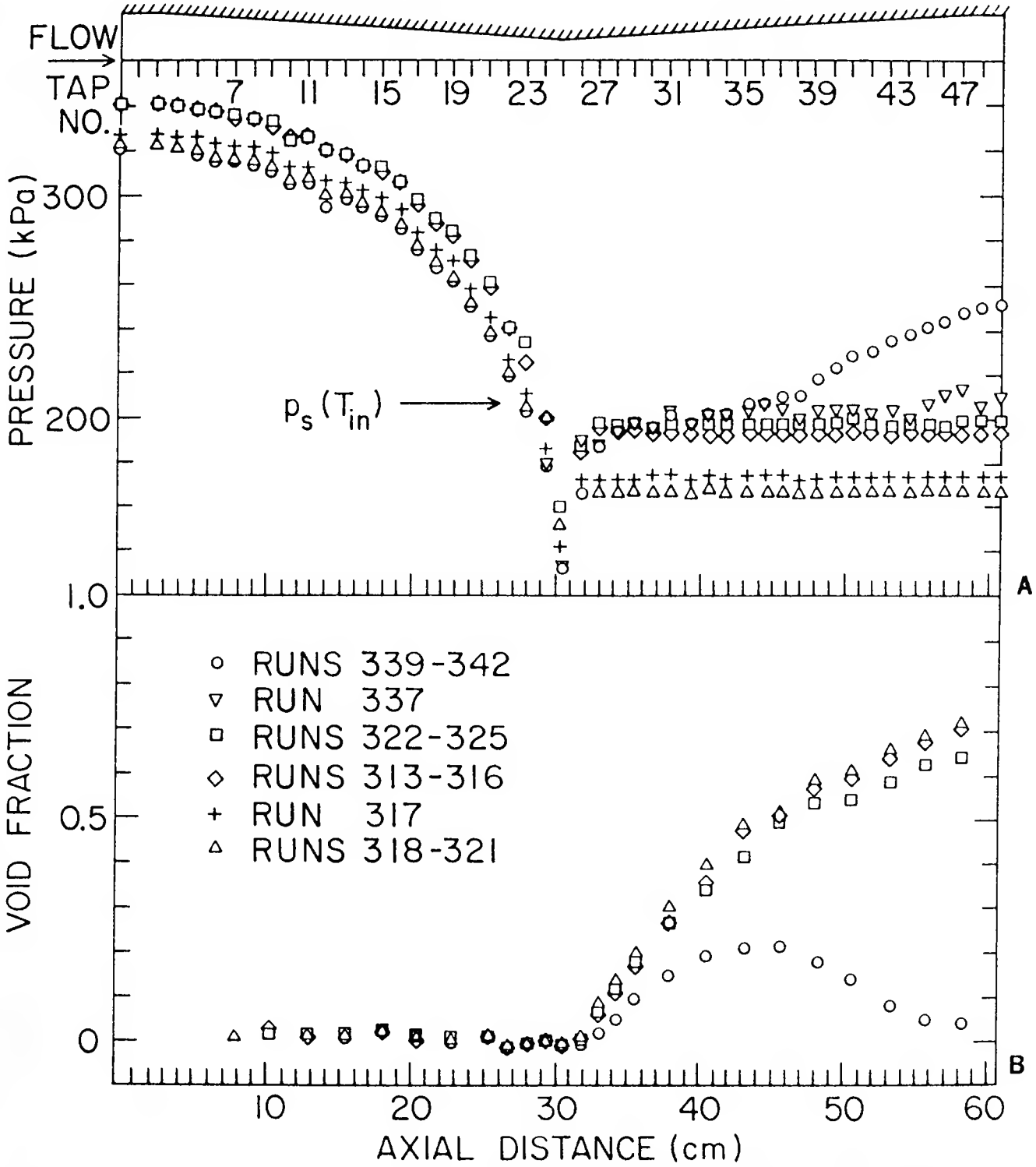

Figure 1.10 Axial Distributions of Pressure (A) and Area Averaged Void Fraction (B) for Runs Performed at an Inlet Temperature of 121°C, a Constant Inlet Mass Flux, and Decreasing Nozzle Exit or Condensing Tank Pressure (BNL Neg. No.9-622-80).

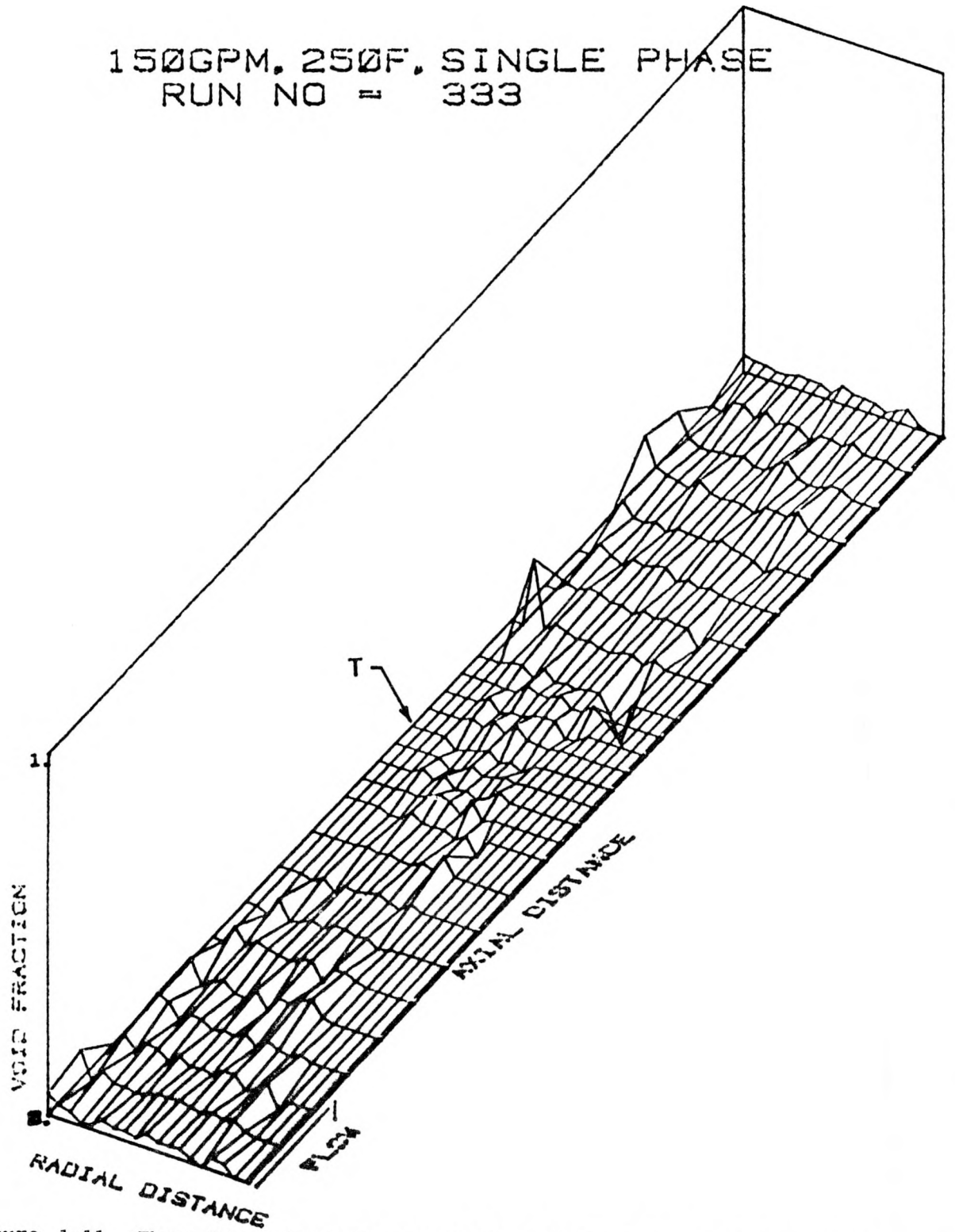

Figure 1.11 Three Dimensional Representation of the Chordal Averaged Void Fraction Distributions Along the Test Section (T Designates the Nozzle Throat) (BNL Neg. No. 9-600-80).

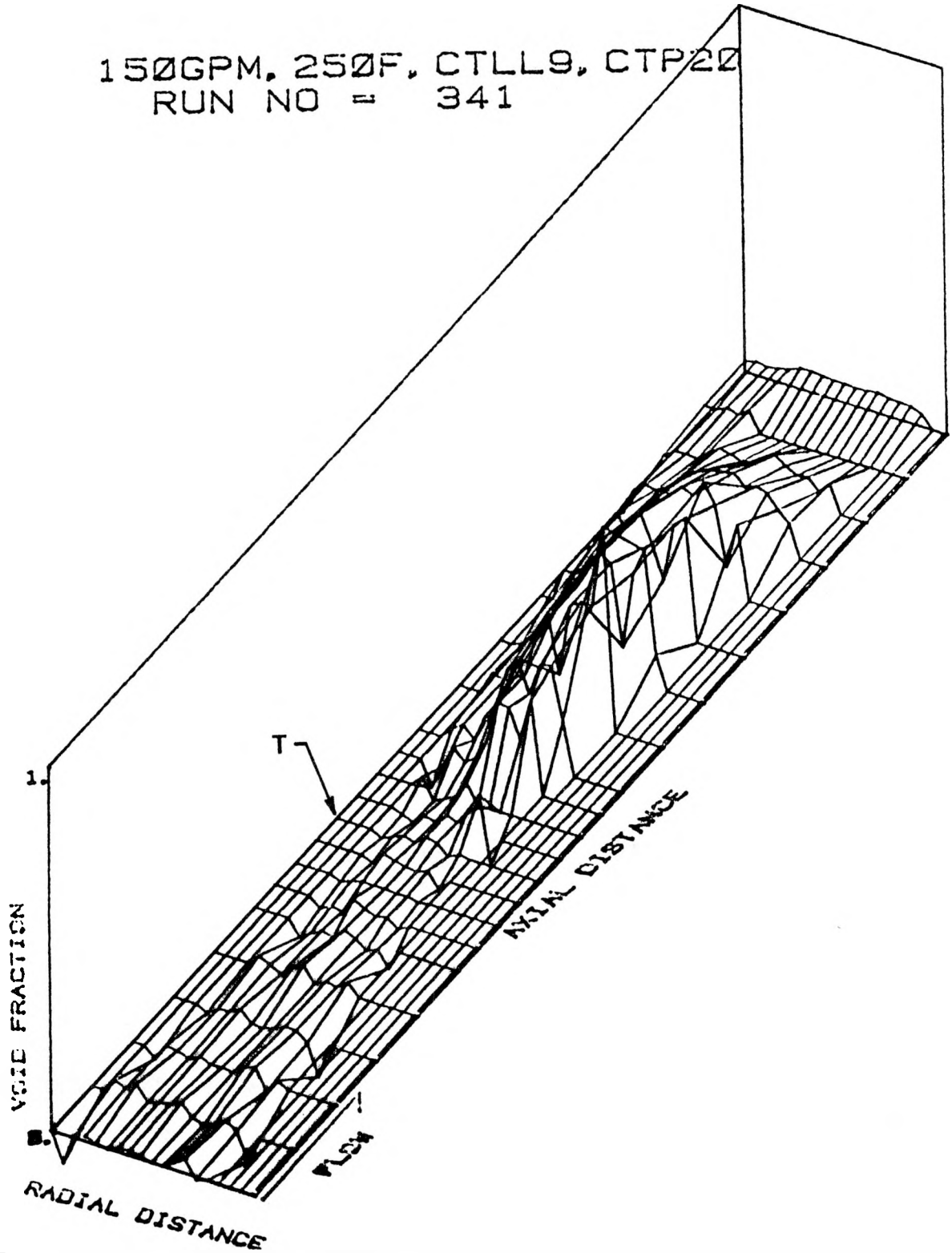

Figure 1.12 Three Dimensional Representation of the Chordal Averaged Void Fraction Distributions Along the Test Section (T Designates the Nozzle Throat) (BNL Neg. No. 9-593-80).

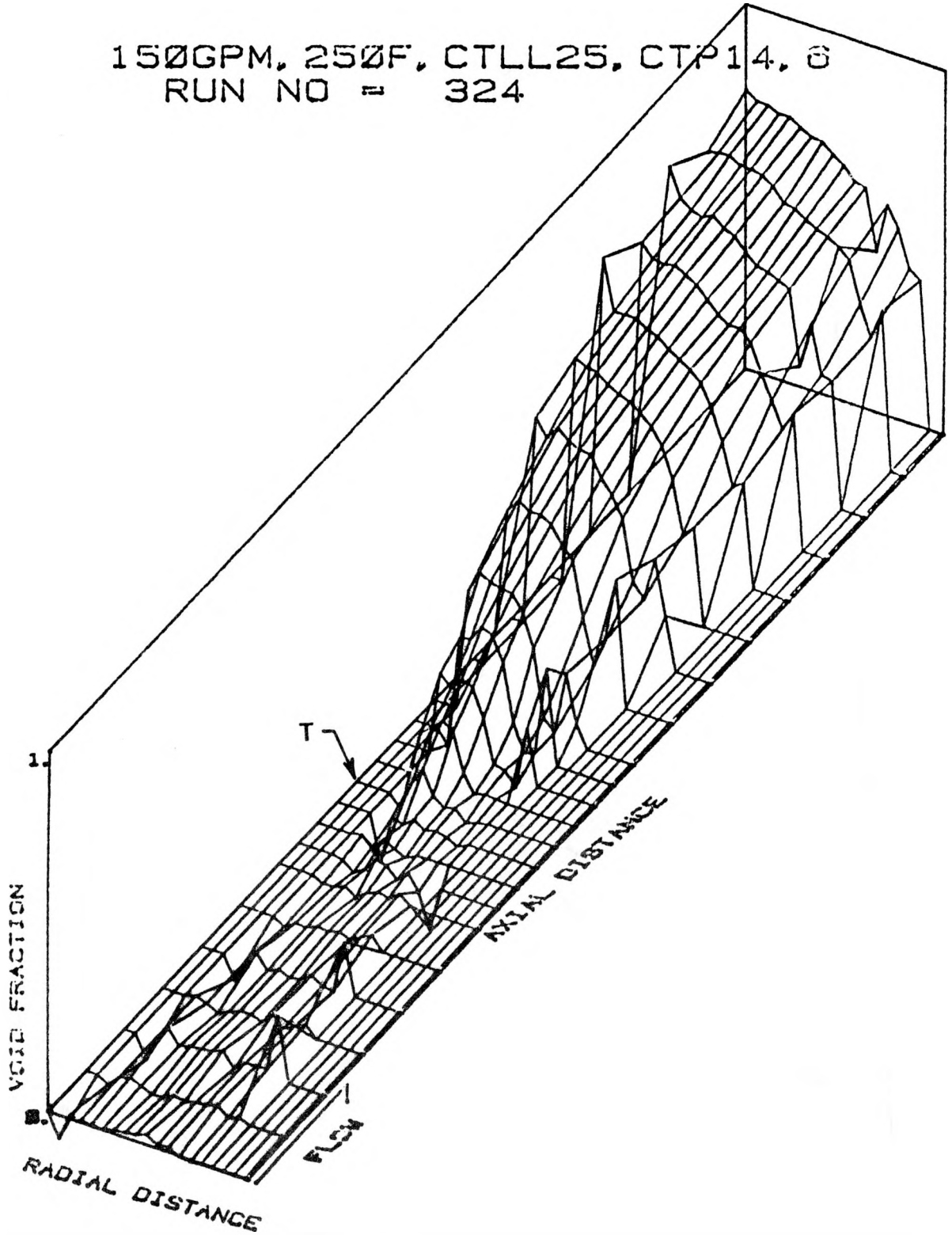

Figure 1.13 Three Dimensional Representation of the Chordal Averaged Void Fraction Distributions Along the Test Section (T Designates the Nozzle Throat) (BNL Neg. No. 9-594-80).

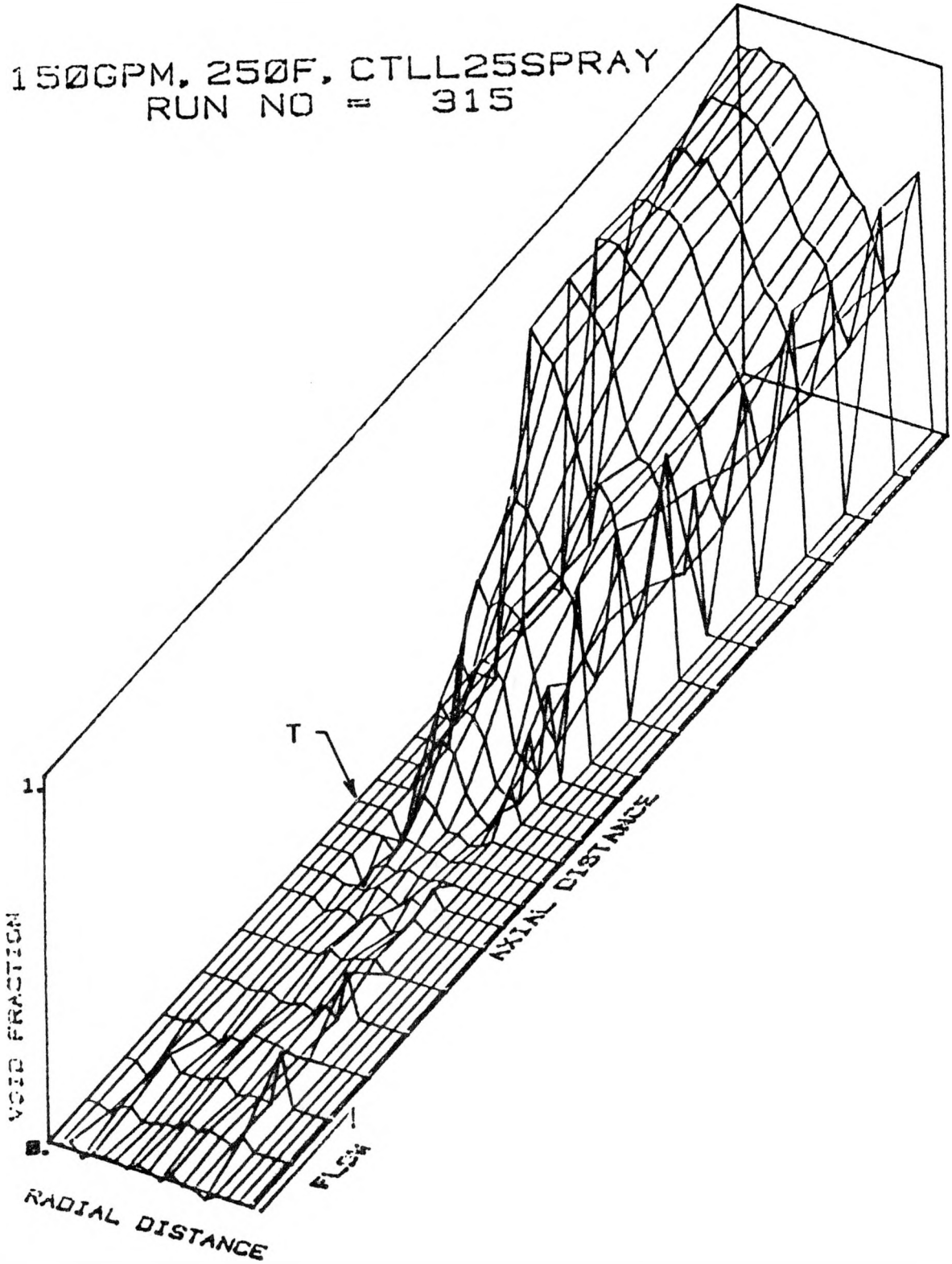

Figure 1.14 Three Dimensional Representation of the Chordal Averaged Void Fraction Distributions Along the Test Section (T Designates the Nozzle Throat) (BNL Neg. No. 9-602-80).

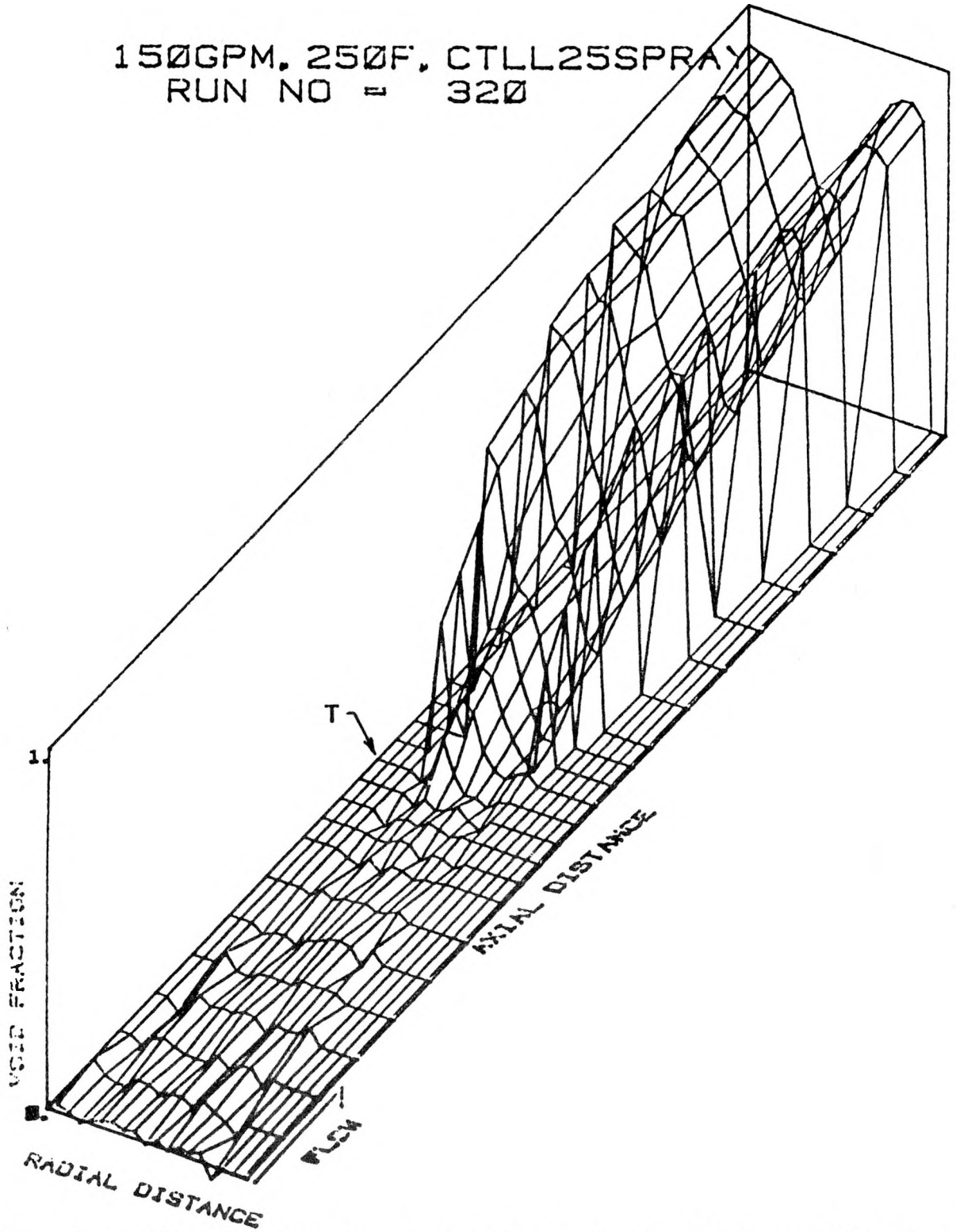

Figure 1.15 Three Dimensional Representation of the Chordal Averaged Void Fraction Distributions Along the Test Section (T Designates the Nozzle Throat) (BNL Neg. No. 9-597-80).

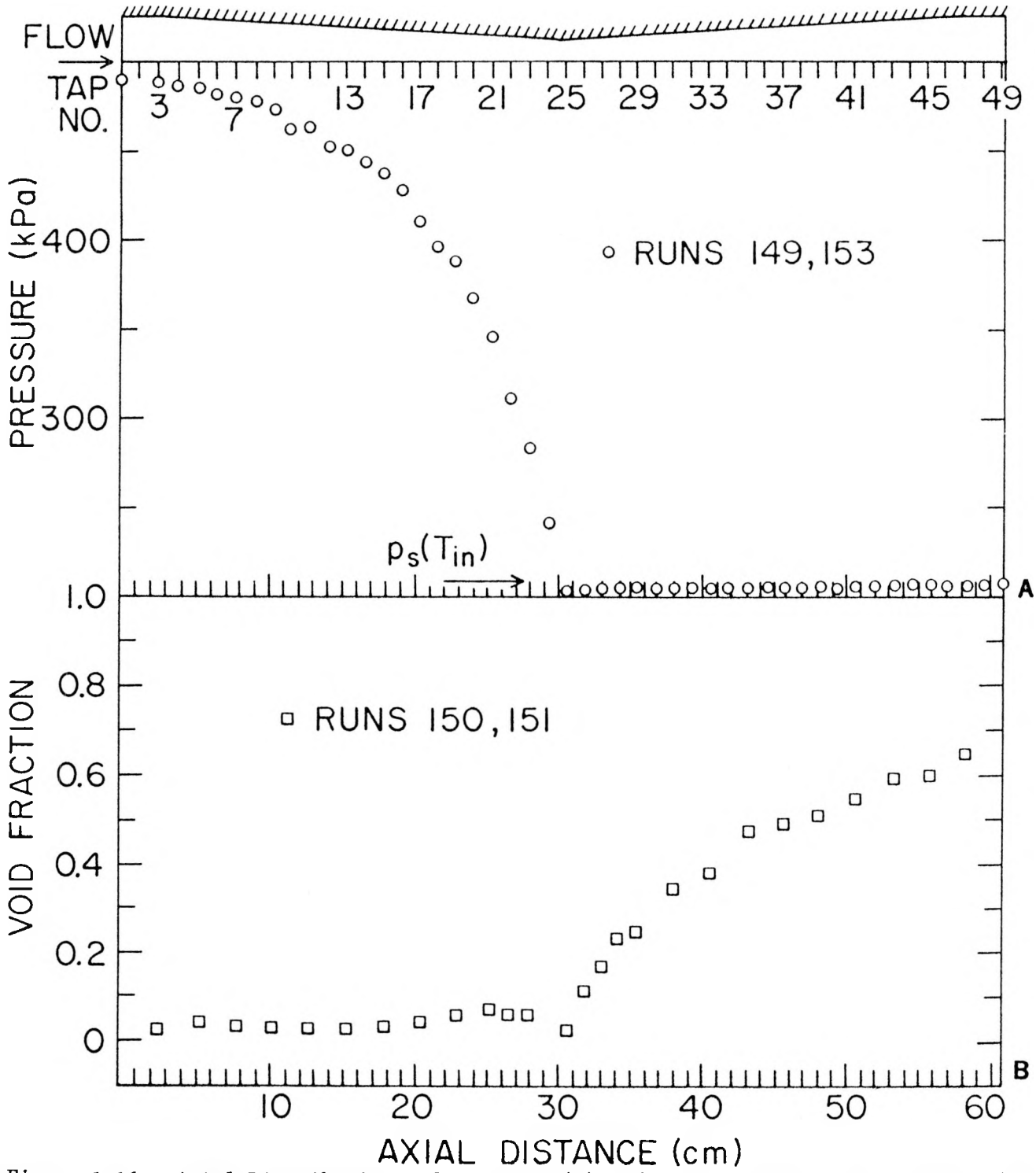

Figure 1.16 Axial Distributions of Pressure (A) and Area Averaged Void Fraction (B) for Runs 149-153, Performed at an Inlet Temperature of 121°C with MgO Particulates Present in the Water Loop (BNL Neg. No. 9-626-80).

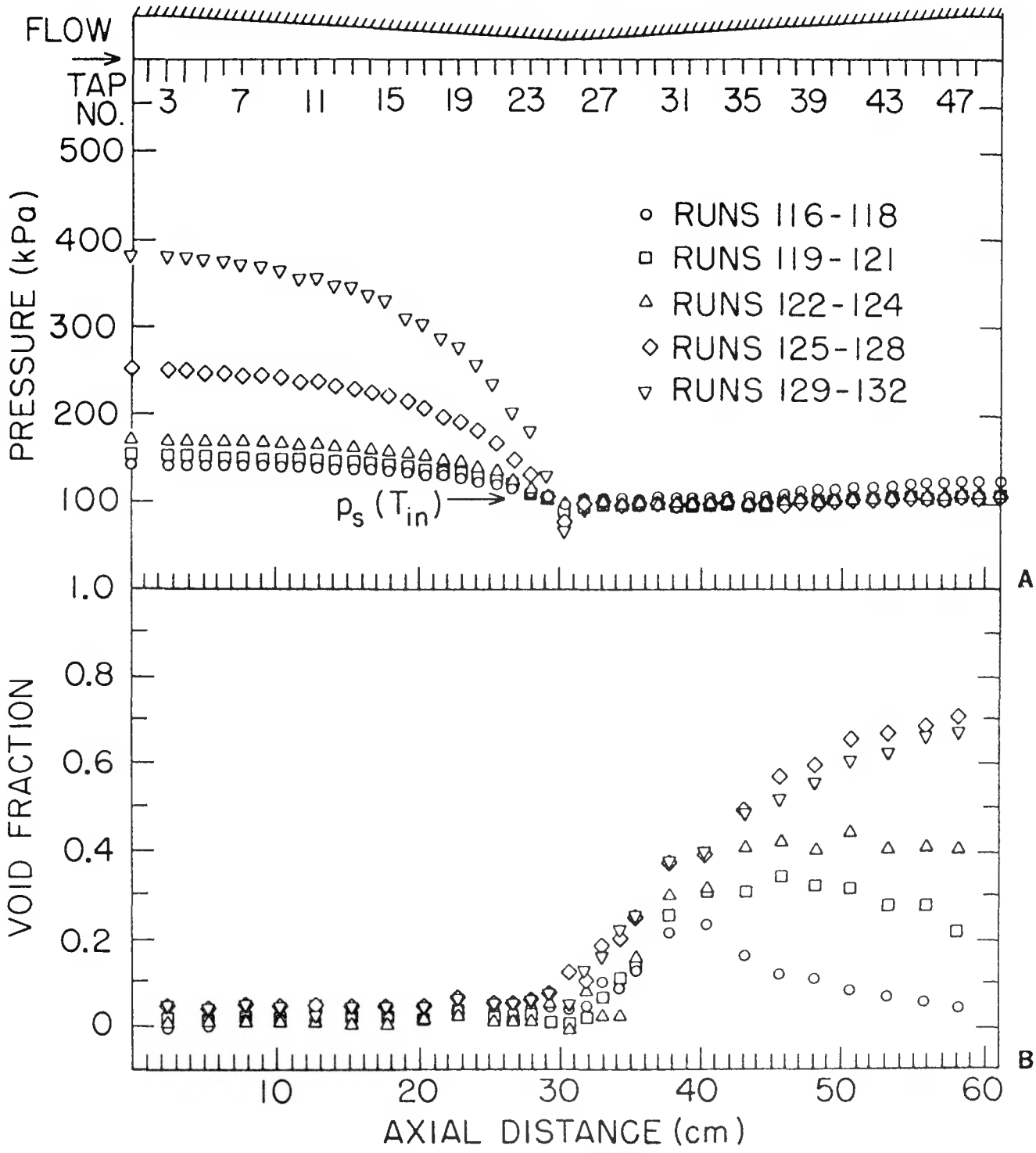

Figure 1.17 Axial Distributions of Pressure (A) and Area Averaged Void Fraction (B) for Five Runs Performed at an Inlet Temperature of 100°C and Increasing Inlet Mass Fluxes (Five Beam Gamma Densitometer) (BNL Neg. No.9-636-80).

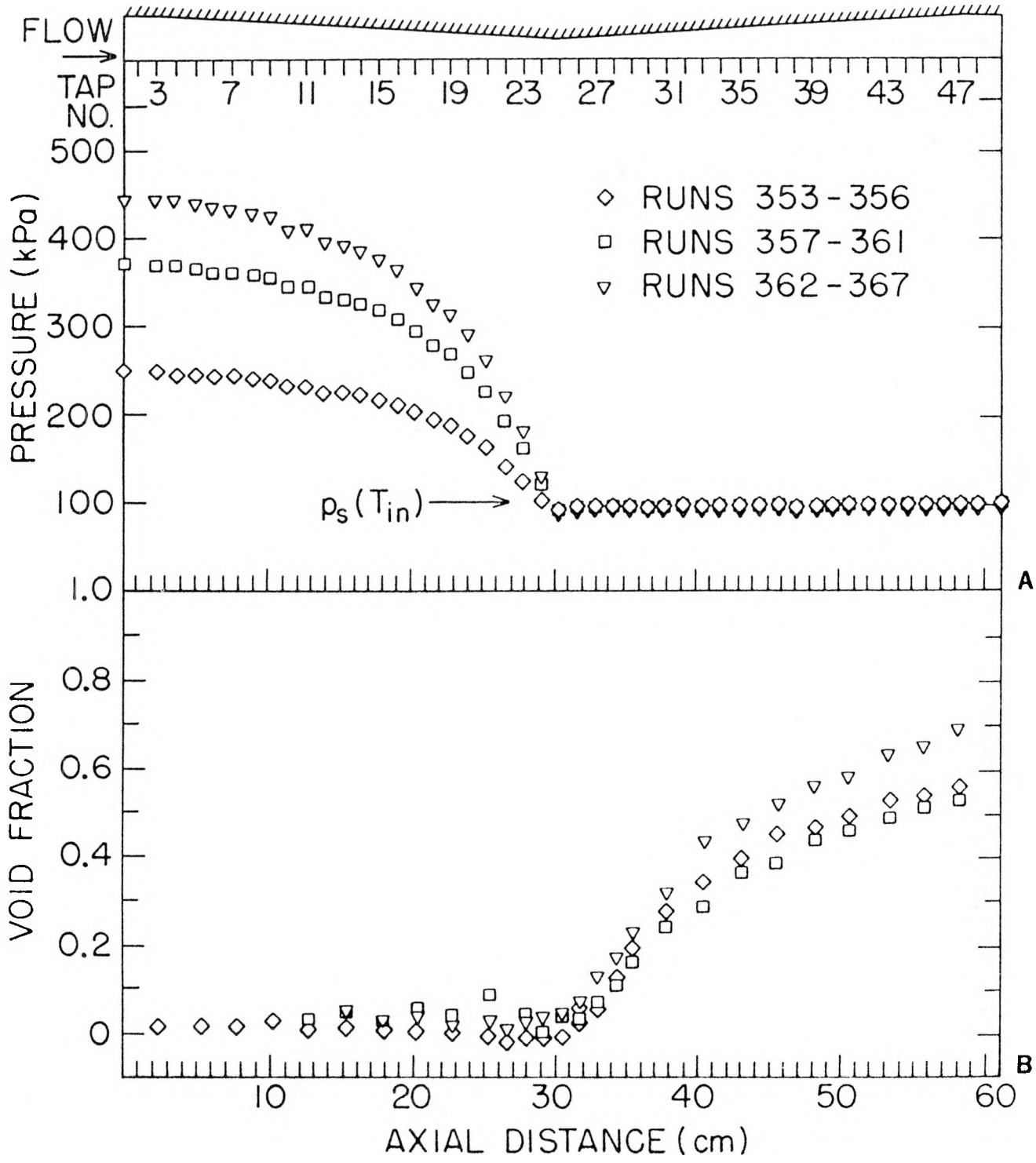

Figure 1.18 Axial Distributions of Pressure (A) and Area Averaged Void Fraction (B) for Three Runs Performed with the High Activity Single Beam Densitometer, at an Inlet Temperature of 100°C, and Increasing Inlet Mass Fluxes (BNL Neg. No. 9-643-80).

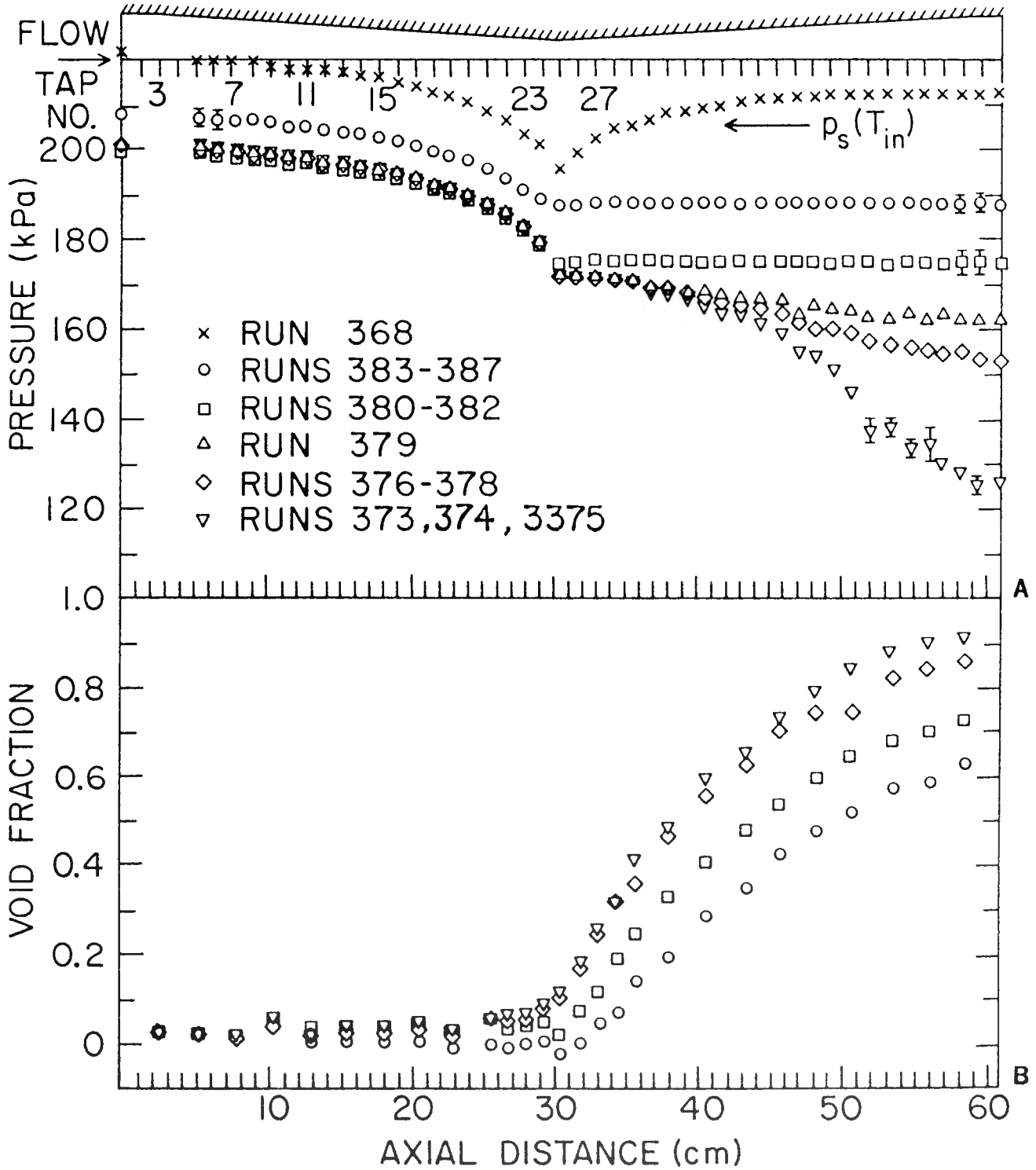

Figure 1.19 Axial Distributions of Pressure (A) and Area Averaged Void Fraction (B) for Several Runs Performed at an Inlet Temperature of 121°C and Single and Two-Phase Inlet Conditions (BNL Neg. No.9-628-80).

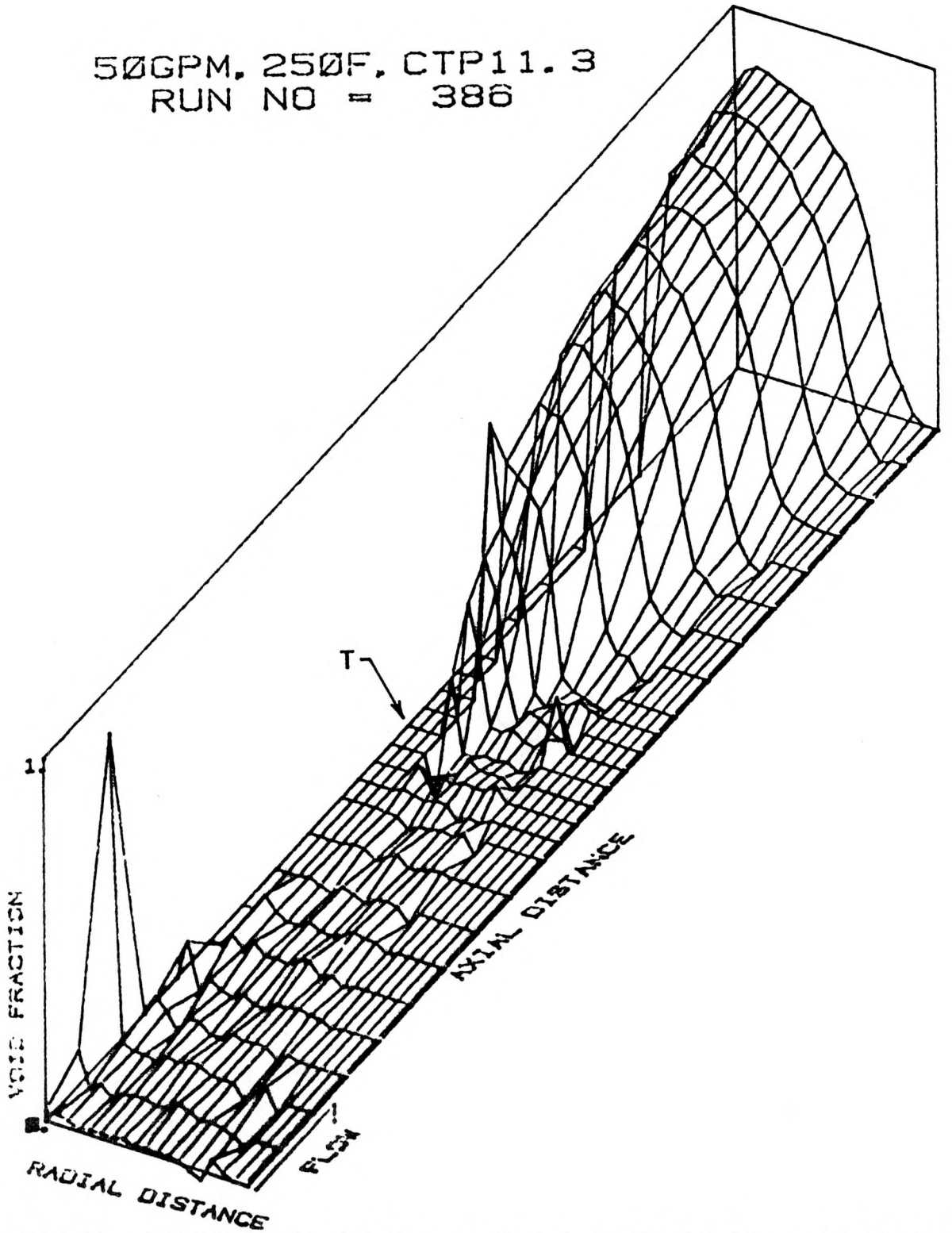

Figure 1.20 Three Dimensional Representation of the Chordal Averaged Void Fraction Distributions Along the Test Section (T Designates the Nozzle Throat) (BNL Neg. No. 9-596-80).

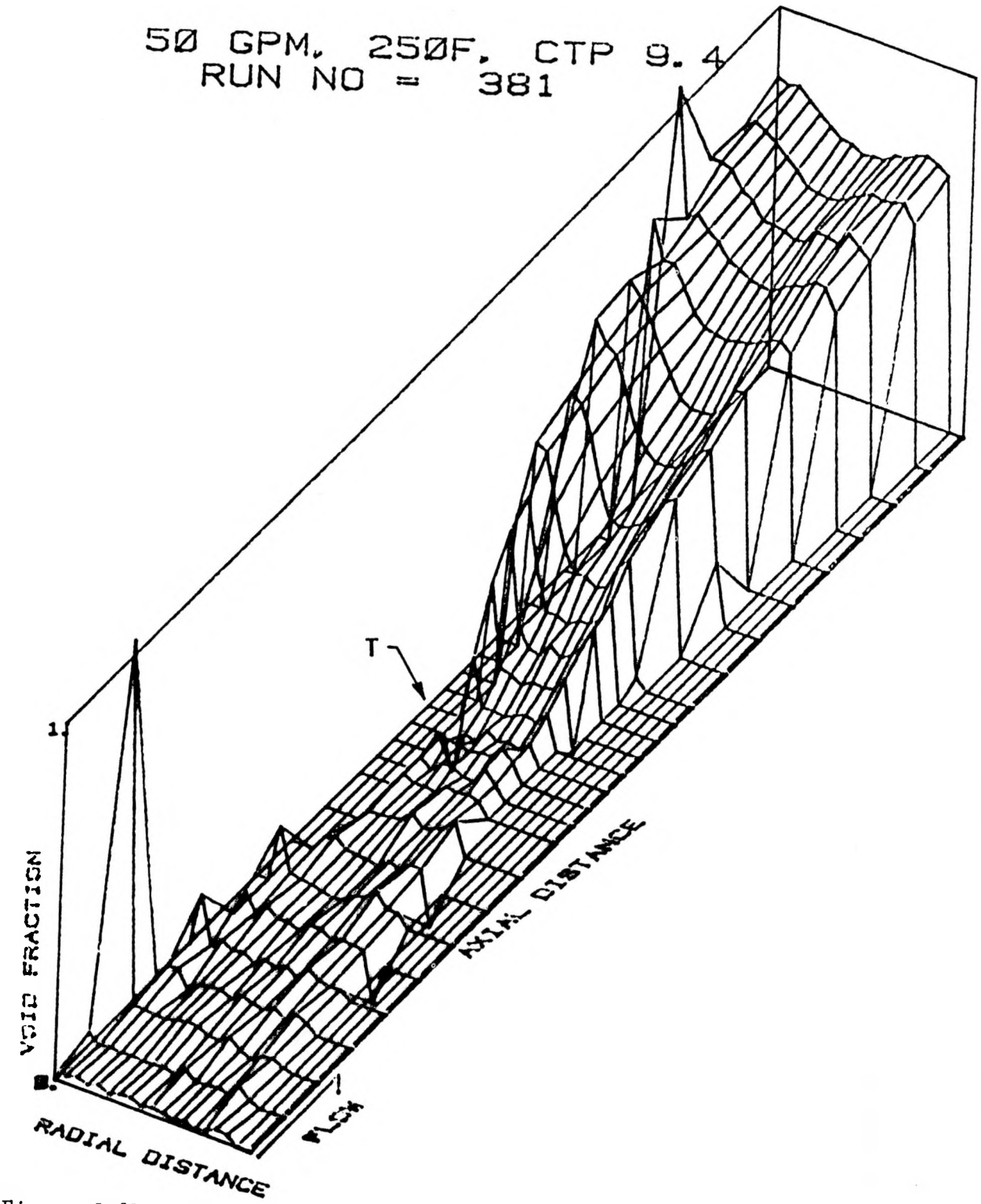

Figure 1.21 Three Dimensional Representation of the Chordal Averaged Void Fraction Distributions Along the Test Section (T Designates the Nozzle Throat). (BNL Neg. No. 9-595-80).

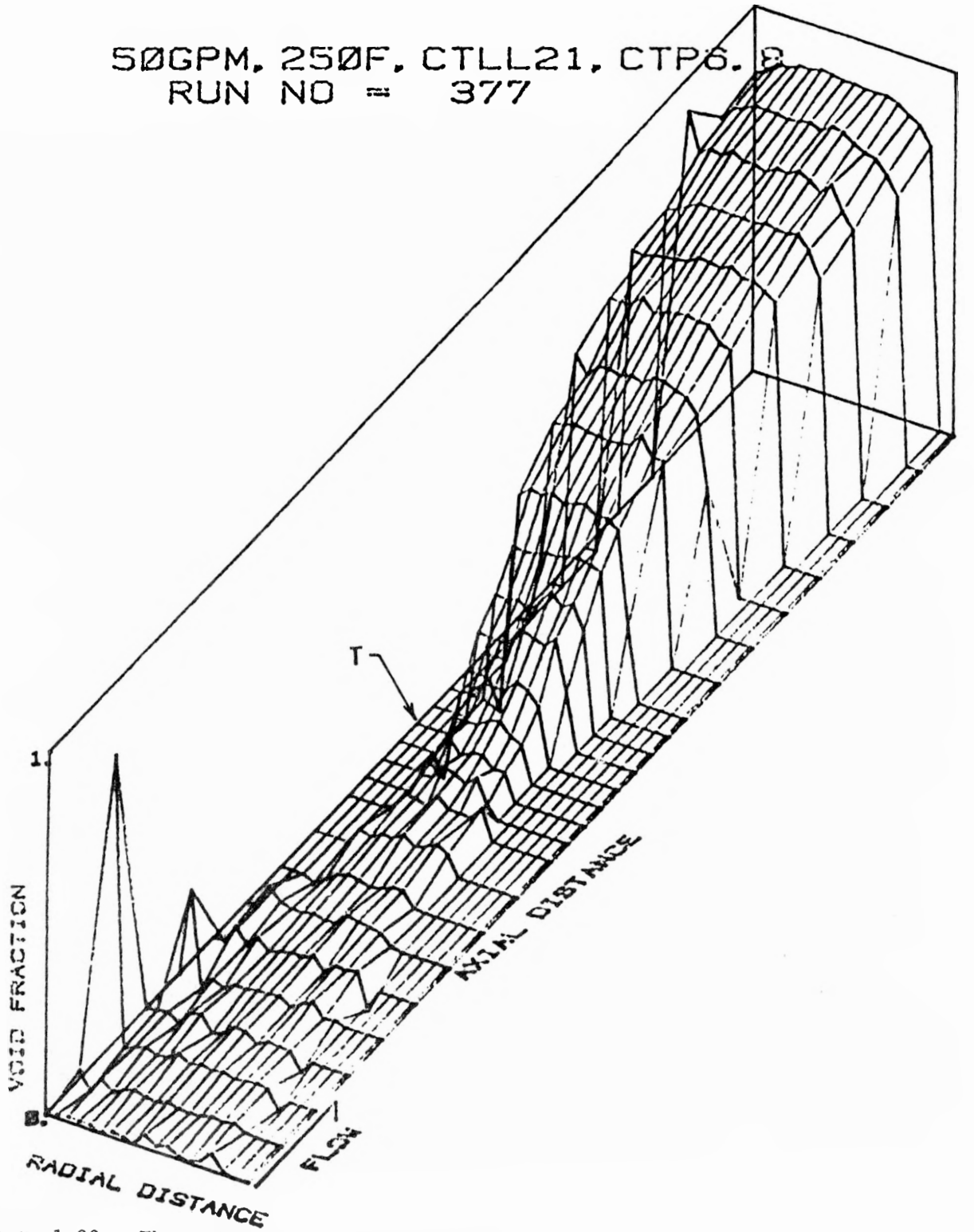

Figure 1.22 Three Dimensional Representation of the Chordal Averaged Void Fraction Distributions Along the Test Section (T Designates the Nozzle Throat). (BNL Neg. No. 9-598-80).

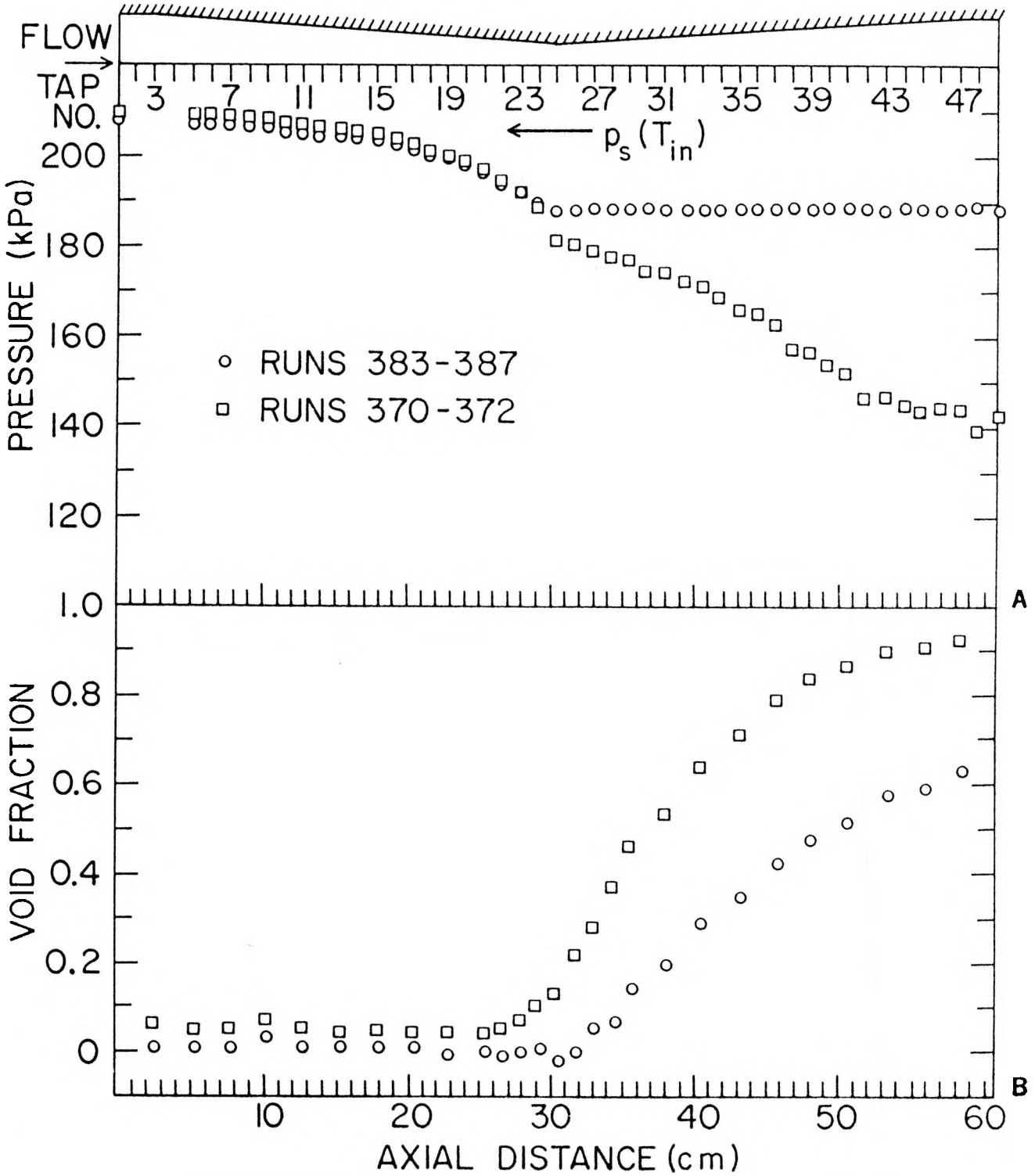

Figure 1.23 **Axial Distributions of Pressure (A) and Area Averaged Void Fraction (B) for Two Runs Performed at Similar Inlet Conditions and Varying the Condensing Tank Pressure. (BNL Neg. No. 9-623-80).**

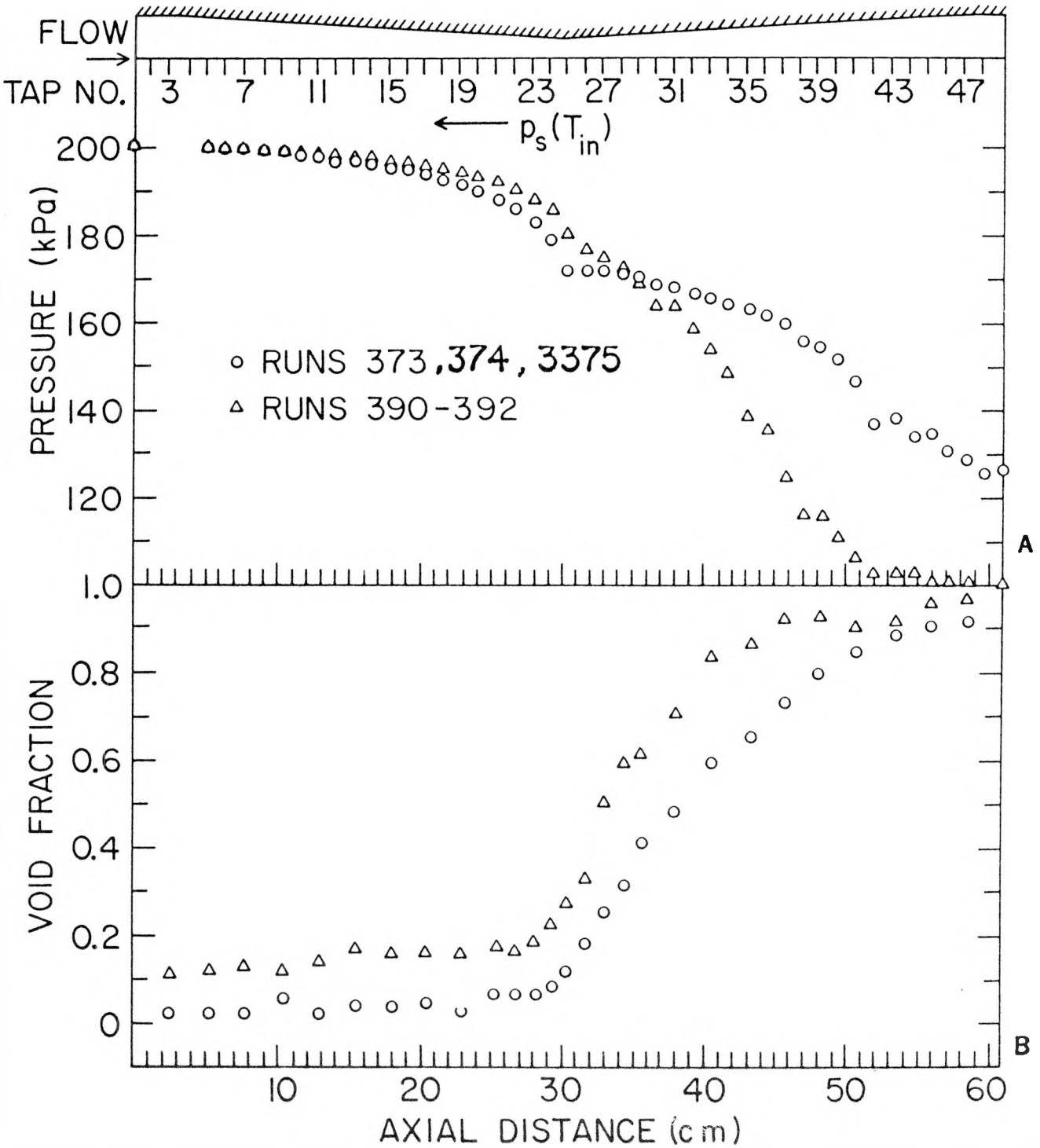

Figure 1.24 Axial Distributions of Pressure (A) and Area Averaged Void Fraction (B) for Two Runs Performed at an Inlet Temperature of 121°C, Two-Phase Inlet Conditions,, and at Two Inlet Mass Fluxes of 1510 kg/m^{2}s (Runs 373, 374, 3375) and of 1065 kg/m^{2}s (Runs 390-392). (BNL Neg. No. 9-625-80).

2.0 RAMONA-III Code Modification and Evaluation

(D. J. Diamond, D. Garber, S. V. Lekach, C. J. Ruger)

In the last quarterly progress report (Diamond, 1980) the requirements for a code which can calculate small pipe break (SPB) loss-of-coolant accidents for a BWR were discussed and tests, additions and modifications were proposed for RAMONA-III. During this reporting period a number of these items were examined namely:

(1) Level tracking as applied to the downcomers.
(2) Void profile in the core-riser as it applies to representing a level.
(3) Reverse flow.
(4) Two-phase flow in downcomers.
(5) Running times.
(6) Core spray modeling (i.e. cold water injection).
(7) Optional removal of neutronics to increase computation speed.

Throughout these investigations attempts were made to focus on areas which bear on modeling SPBLOCA and to identify and if possible resolve any problem areas within the time frame allowed. A simplified reactor model of the Peach Bottom-II plant was used in this work. It consisted of four neutronic channels and three hydraulic channels (including bypass) in the core.

A water level tracking logic is presently installed to track levels in the downcomers. The logic seems to be working over the relevant range of levels in the downcomer.

Numerous runs have been made in an attempt to create and then study a core water "level". What is meant by "level" is an abrupt increase in void fraction approaching 1.0 with an associated decrease in liquid velocity. Numerous runs have been made under the following conditions:

(1) holding pressure temporarily constant
(2) scramming control rods and adjusting decay heat
(3) reducing inventory by implementing a negative feedwater flow, and
(4) reducing the pump head to reduce flow velocity in core.

Difficulties have been encountered in establishing the sharp "level" being sought. The intrinsic limitations of the RAMONA-III code modeling have not yet been tested. The difficulties encountered to date relate to limitations in the FORTRAN logic associated with running the code in new areas and complications introduced by the bypass channel.

Tests have been constructed to exercise the code's ability to compute reverse flow. Reverse flow has been observed from the mid-core region down through the lower plena and up through the downcomers. There is reason to believe that the code cannot presently model reverse flow in the riser region.

Tests have been constructed to demonstrate that two-phase flow phenomena are being computed in the downcomer regions. Vapor generation, voids, superheat have all been observed and seem to be working.

A number of timing tests have been performed. For the most interesting case in SPBLOCA RAMONA-III seems to be capable of running in real time.

The cold water ECCS injection into the riser has been modeled and implemented in RAMONA-III. The ability to inject cold water into moderately high-void superheated vapor without problems seems to have been achieved.

An option which would allow suppression of the neutronic computation and replacement by tables of heat generation rate vs. time has been implemented. This option is directed at improving running time once the reactor has been fully scrammed.

As a byproduct of the above testing, the code now has the cability to represent a pipe break at the feedwater inlet and a source of ECC water in the riser (core spray).

In addition to the SPBLOCA effort, support was provided in two applications of RAMONA-III of interest in the licensing review process. To assist users of the code, a report is being prepared which describes the code's capabilities and preparation of required input data.

2.1 Level Tracking in the Downcomer

The RAMONA-III code (Øye, 1977) contains logic which will track a water level in either the upper plenum or the downcomers. A single number WLEW is printed. If positive, the level is in the upper plenum; if negative, the level is in the downcomer. The level is computed by determining (a) the total vapor in the system from an overall system balance (b) determining the vapor present in the system away from the level area by summing over all the nodes internal to the system, (c) determining the vapor present in the level area by taking the difference of (a) and (b), and finally (d) determining a level position to account for the residue vapor. (This is not a collapsed level approach.) The values of void used in the summation (b) are those presently defined in the problem. The void fractions utilized in the calculation in the level region are assumed to be 1.0 above the level and possibly non-zero below (taken from nodes further below the level).

Tests were made to exercise the downcomer level tracking logic. Modifications were made to RAMONA-III to allow outward feedwater flow. This involved accounting for enthalpy other than that associated with the imposed input feedwater temperature for the outward flow case. Problems were encountered in the level track logic in the subroutine HYDRO1 which could not handle level rise following level fall (i.e. level retreat). The problem was created by nodes which had previously been above the level reentering the level track logic with a void fraction of 1.0; this also was fixed. Tests have been run which initialize the steady state level 3 meters below the downcomer top. The feedwater rate is increased and the water level is seen to fill the downcomer and enter the upper plenum. With a negative feedwater, the level has been seen to fall and then rise when the pump is rapidly shut down.

Minor problems still remain in the level logic. The feedwater energy flux is omitted when the water level is below the feedwater node. When the level is below the node associated with the pump, the pump ceases to be in the problem.

During SPBLOCA, water level indicators located in the downcomers play an important role in activating control systems. The water level tracking logic

appears to be working over the relevant range of levels in the downcomer.

2.2 Void Profile and Level Tracking in the Core

The RAMONA-III code presently computes a variety of two-phase quantities for the reactor problem being modeled. In the core the mesh being utilized is 24 axial nodes. Each mesh interval corresponds to a 6 inch length. At each of these discrete mesh points values of void fraction, water temperature, vapor generation rate, liquid velocity, and slip, (which gives gas phase velocity) are computed. Fissions from the neutronics deposit energy directly into the water and into the fuel with subsequent heat transfer to the water. At present, only two heat transfer regimes are modeled, boiling and non-boiling. Each node is considered to be entirely in one or the other heat transfer regime.

During small pipe break LOCA, a loss of liquid inventory is expected. Under some circumstances a "level" is envisioned to drop into the core-riser region. The core does not have level detectors for reactor control as does the downcomer; interest in the core "level" is through the need for introduction of additional heat transfer regimes.

A series of runs have been made to first establish a "level" in the core and then study it. What is meant by "level" is an abrupt increase in void approaching 1.0 with an associated decrease in liquid velocity approaching the "level" movement velocity. To produce this step in void from 0 to 1 over a short axial distance, which could be maintained in time, low liquid velocities were sought (like pool boiling). When the liquid velocity is high, a rapid increase in void fraction over a short distance implies a strong localized vapor generation rate.

It has been noted that finite slip values tend to maintain or increase liquid velocities as the void is increased. The slip correlation used is the Bankoff-Jones correlation which is well behaved over the entire range of void (0 to 1). (The Bankoff-Malnes correlation in the code is also protected over the entire range of void.)

Runs were made under the following conditions: (1) system pressure kept constant, (2) control rods scrammed, (3) feedwater flow direction reversed, and (4) rapid reduction of the circulating pump speed. Holding the system pressure constant was an initial step until a maintainable level was observed. At that point a rapid decrease in pressure was imposed to study the level swell scenario. The control rods were scrammed and within 2-3 seconds the reactor power was at the decay heat asymptote. Runs have been made which artificially impose a zero decay heat limit to better simulate a pool boiling situation. The feedwater reversal was the mechanism to decrease liquid inventory in the reactor. RAMONA-III was modified to allow a negative feedwater flow which was removed at a rate between 1 and 5 times the steady state input rate (1140 kg/sec). Finally, the pump head was decreased by ramping down the circulation pump speed. The pump head was decreased for two reasons. The pump head causes the core "level" to be higher than the downcomer level and an observable level in the core is being sought. The pump head is also a major controller of the flow through the core and low flow velocities are being pursued.

A number of minor problems were encountered in these runs since RAMONA-III was being exercised in new untried areas. Low flow velocities into the core were obtained and a variation of void fraction from 0 to 0.74 over six nodes was observed. The void asymptote of 0.74 continued up through the riser. At that moment the level in the downcomer was 2.5 meters above the top of the core. This void step is considered not to be the "level" associated with exhausting the water inventory but rather with a peak in heat flux and vapor generation rate which occur at these positions.

The bypass channel in the core has lower flow velocities than the in-channel paths. In the attempt to obtain lower flow velocities, stagnation occurs in the bypass channel which leads to reverse flow. The subsequent flow pattern did not lead to a situation where conclusions can be made about levels.

Difficulties have been encountered in establishing the sharp "level" being sought. The intrinsic limitations of the RAMONA-III code modeling have not yet been tested. The difficulties encountered to date relate to limitations of FORTRAN logic encountered in running in new areas and complications introduced by the bypass channel.

2.3 Reverse Flow

The question as to whether RAMONA-III can handle reverse flow has been investigated. Reverse flow occurs when the liquid (or mixture) velocity is in a direction opposite to that found in steady state such as can occur following a SPBLOCA. These conditions were simulated by scramming the reactor, rapidly decreasing the recirculation pump speed, and decreasing the decay heat until the water velocity in the core was decreased to quite low values. Stagnation was obtained in the bypass channel producing upward flow in the top and downward flow in the bypass bottom. Vapor generation at the stagnation point causes increased downward flow which ultimately produces a net downward flow through the lower plena and upward through the downcomers.

Another run which involved rapid removal of a control rod causing a huge power spike produced similar reverse flow in the lower regions of the core channels. It should be noted that in both cases studied the flow was always positive in the upper core regions. It is believed by Scandpower (and BNL) that the present logic in the core outlet-riser inlet is not adequate to handle reverse flow. This is related to the code's inability to distribute flow into multiple core channels from the riser.

While countercurrent flow is not reverse flow, it is of interest to note that negative values of slip have been observed. RAMONA-III computes the vapor velocity from the slip correlation value times liquid velocity plus the bubble rise velocity. In the case of a small negative liquid velocity it is possible to have a positive gas velocity and this has been observed.

2.4 Two-Phase Flow in Downcomers

The question as to whether RAMONA-III can handle two-phase flow phenomena in the downcomer has been asked and addressed. A number of cases have been

run where non-zero values of void fraction, evaporation/condensation, and temperatures other than saturation have been observed. The case most relevant to SPBLOCA was that of an overall system depressurization of 0.18 MPa/s which produced superheating of the order of 0.6°C and evaporation rates of 3 kg/m^3-s in the downcomers. Two-phase effects were also observed in the lower plena.

2.5 Running Time of RAMONA-III

Since SPBLOCA are transients that can be of long duration, the running time of RAMONA-III is of much interest. To quote meaningful estimates of running time is difficult normally and especially complex in the case of RAMONA-III. The RAMONA-III code allows the neutronics and hydraulics to run at different time steps. The neutronic time step, which is always larger than the hydraulic time step, is controlled by the temporal variation of fast neutron flux. The hydraulics generally takes many steps for each neutronic step, and has its time step controlled by a complicated algorithm reflecting stability and truncation time step limits. Within each calculation there exist iterative components which contribute to the computational work which indicate the degree by which the present state departs from the previous state.

With these ideas in mind a number of runs attempting to simulate SPBLOCA were made. Runs with a quarter core representation of the Peach Bottom-2 vessel were made with: 191 neutronic channels and 31 hydraulic channels, 4 neutronic and 3 hydraulic channels, and 4 neutronic and 3 hydraulic channels but modified to allow the neutronic time step to increase to 1.0 second. These runs all involved scramming the reactor and withdrawing water from the feedwater pipe to simulate a leak. During the early part of the transient while the control rods are moving the computational work (in 7600 CPU-seconds/second of transient/neutronic or hydraulic 24-axial node channel being modelled) was the same for the neutronics and hydraulic computations (2 or 5 CPUsec/sec/channel depending on the version of the code used). The duration of scram took between 2-3 s of reactor time when the neutronics approached the decay heat asymptote. (Note: in the present version decay heat is a constant.)

Of more interest for assessing run time for SPBLOCA is the transient when the reactor is no longer critical. With the code version which can attain large time steps, the hydraulic computation proceeded at 0.4 CPUsec/sec/channel with the neutronic times being 0.06 CPUsec/sec/channel. The fractional computation time which is "neutronics" (15%) includes the fuel heat transfer computation which is still required during SPBLOCA. It is concluded from these results that once the initial scram of 2-3 s is over, a coarsely represented reactor can be modelled by RAMONA-III in real time. (Model includes downcomer 1 and 2, lower plenum 1 and 2, core with 24 axial nodes/channel, riser, and upper plenum.)

Also of interest in this area of run time is the problem of time step control. In an indirect way RAMONA-III uses the void feedback and neutronic time step control to control the hydraulic time step size. With the neutronics scrammed, problems were encountered in obtaining convergence in void fraction (i.e. exceeding iteration limits). The riser inlet is sensitive to changes in the reactor hydraulics since disturbances propagate through the

core and bypass channels at different rates. The time step control needs modification to anticipate reaching iteration limits in the hydraulics.

2.6 ECCS Modeling (Cold Water Injection)

To calculate small break LOCA transients the RAMONA-III code must be able to model the Emergency Core Cooling Systems (ECCS). Two of these systems are the High Pressure Core Spray (HPCS) and the Low Presssure Core Spray (LPCS) systems. These systems supply cold water from the suppression pool to a spray header in the reactor pressure vessel above the core. This corresponds to the riser loop part in the RAMONA-III Code. At the time during a SBLOCA that these systems begin injection of cold water the void fraction (α) in the riser can be quite high even approaching pure steam ($\alpha = 1.0$). The temperature of this high void flow will be near saturation (assumed for the vapor phase), which is much higher than that of the suppression pool (ambient temperature). This raises the question of whether the RAMONA-III code is capable of calculating the mixing of these vastly different temperature flows and the associated condensation in the two-phase mixture at specific source node in the riser used to model the HPCS/LPCS injection.

To effectively test the cold water injection capability of the code a source node was added to the riser loop part of the RAMONA-III code. In order to add this source node a study was made of the feedwater flow introduction coding for the existing code. The feedwater inlet is restricted to the downcomers and lower plena. However, the basic modeling would be the same for the riser. The coding logic for the feedwater is extremely complex, especially for the integrated momentum equation.

For an initial checkout of the cold water injection capability a constant injected mass flow and constant injectant temperature were used. Since the injected water is obtained from the suppression pool a temperature of 40°C was used for all cases. All cases used a system pressure of 69.8 bar yielding a saturation temperature of 285.6°C. Thus, the injected water is about 245°C colder than the main flow, which is close to saturation in the riser. For all calculations the first node in the riser above the core-riser interface was chosen as the injection point.

The test cases were computed by suddenly injecting this cold water at an arbitrary time during test runs being made for level tracking testing, (see above). These calculations use various artificial means to obtain high core void fractions. In the first case an injected mass flow of 200 kg/s is added to a main flow of 1.31×10^4 kg/s; a ratio of 1.5%. At the time of injection initiation, the riser void fraction varied from 0.531 at the entrance to 0.535 at the exit. The flow was slightly superheated at the entrance (0.4°C) and saturated at the exit. The corresponding evaporation rates varied from $\psi = 5.6$ to 0.0 kg/s-m^3. At the next time step, 0.02 s, the flow at the injection point began to condense, $\psi = -0.61$kg/s-m^3, and became subcooled, 0.12°C. After 0.2 s of injection the entire riser above the injection point exhibited condensation and subcooled flow. The riser void profile showed a corresponding void collapse at the injection point with $\alpha = 0.536$ at the entrance, $\alpha = 0.525$ at the injection node and then increasing to 0.535 at the riser exit. The riser water velocity is about 3.0 m/s indicating that the same fluid remains in the riser and the effect of the cold water is diffusing

upward as calculated. It should be noted that in all cases a transient is under way due to other disturbances and the effect of this injection is superimposed on the other effects. This case was run for another 12 s without any change in the trends from when the ratio of injected-to-main flow was 1.5%.

In a second case the same 200 kg/s injectant is introduced to a main flow of 2.96 x 10^3kg/sec, a 6.7% ratio. The riser entrance void fraction was 0.626 decreasing to 0.542 at the exit. The results were very similar to the first case with the first condensation after 0.05 s and condensation at the riser exit after 0.23 sec.

In the third case the injected mass flow was increased to 1000 kg/s yielding an injectant to main flow ratio of 25.5%. The riser entrance void fraction was 0.621 and 0.542 at the exit. Again the code computed similar results with condensation reaching the riser exit after 0.2 sec. However, the increased injection flow rate causes a more pronounced void collapse at the injection point. For example, after 0.5 s of injection the riser entrance void is 0.755 while the injection point collapses to α = 0.458. The void fraction then increases back to 0.546 at the exit.

In all three cases the code had no difficulty in calculating the injection of water 245°C colder than the main stream at up to 25% of the main stream flow rate. However, the void fractions at the injection point were only of the order of 0.6. To further test the injection capability the injection should occur at a void fraction approaching 1.0. Also the injection should be initiated at a time when the main flow has reached a steady state condition so the effect of the injection can be more readily assessed. As further level tracking test runs reach these conditions additional cold water injection tests will be conducted.

2.7 Input of Power Generation

In its normal operational dynamic mode, RAMONA-III solves the neutronic and the fuel conduction equations for a neutronic time step, and then solves the hydraulic equations for a series of hydraulic steps (a hydraulic step is determined by a stability-truncation error criterion in the code and is always smaller or equal to a neutronic step) until the hydraulic time level reaches the neutronic time level.

During a small break transient calculation the neutronics play a small role because the reactor scrams at the beginning of the transient. In order to speed up the code the neutronics can be replaced by a set of tables that give prompt and delayed nuclear power as a function of time (which will be used by the fuel conduction routines to obtain temperature distributions and power to the coolant).

The code has been modified to bypass (at a specified input time) the routines that calculate both the fast and thermal fluxes, but still uses the fuel conduction routines. The hydraulic routines remain unchanged. The code still uses the same time step control structure in the neutronic section. Even though the flux calculation is bypassed, the neutronic section still is used; it contains the fuel conduction routine TFDYN, the neutronic output routine DYNLIST, and a neutronic predictor routine PREDYN. Neutronic time

step control is still being done as before except that the slopes of the input power tables are being used to predict the fast flux array (which will be used to determine the next neutronic time step).

It was decided not to bypass the steady state neutronic section of the code at this time because of the complicated input required for the delayed and prompt nuclear power distributions everywhere in the 3-dimensional reactor representation. In addition to that, a detailed temperature distribution and power-to-the-coolant distribution would be needed.

Presently, the code calculates the steady state, then proceeds with a normal dynamic calculation until it reaches a neutronic time level TIMEAQ (input). At this time, it starts bypassing the neutronics and uses two tables (fractional delayed nuclear power vs. time and fractional prompt nuclear power vs. time) as a replacement for the neutronics. The fractional powers will be a fraction of powers just before TIMEAQ. Currently the same spatial distribution that existed before TIMEAQ is being preserved; the fraction obtained from the table multiplies all the values in the array. However, it could be modified in the future to account for changes that occur in some part of the core.

The modifications have been checked out by running a typical test reactor transient where a scram occurs, and comparing the results with a version of the code that bypasses the neutronics and uses the delayed and prompt nuclear power tables from the full code version. The code version with power tables gives results that are typically within one percent (for the important parameters) of the full version.

2.8 Plant Input Modelling

Updates have been received from ScandPower which improve the cross section formalism and which transmit the corresponding cross section data for Peach Bottom 2. The improved representation (Moberg, 1980) allows for the void dependence to be a function of burnup and void history; the group 1 fission cross section to be a function of fuel temperature; and the presence of control elements to affect all cross section types. The data supplied for each of three fuel types are at three exposure points and three void history values.

2.9 Applications to Regulatory Problems

Support was given to work being done at BNL for the Division of Systems Integration in the Office of Nuclear Reactor Regulation. A BWR/4 at end-of-cycle, full power operation has been modelled in half-core symmetry in order to calculate "Half-ATWS" for the Reactor Systems Branch. In this transient the main steam isolation valve closes and both scram and recirculation pump trip occur. The scram constitutes only half the control rods.

A steady state BWR/4 model has been set up for a center rod drop accident at zero power for the Core Performance Branch. The cross-section set being used is a beginning-of-life zero power set that had been used previously with the BNL-TWIGL and MEKIN-B codes to analyze the rod drop accident. A Sequence-A control rod pattern is being used. A converged steady state solution has been obtained. Fine tuning of the control rod pattern to maximize

the accident rod worth, and of thermal hydraulic parameters is continuing. A modification was made so that the code would allow for a control rod movement and scram independent of one another.

REFERENCES

D. J. Diamond, et al., Water Reactor Safety Research Division, Quarterly Progress Report, April 1 - June 30, 1980, In press (1980).

L. Moberg, "Improved Cross Section Representation in RAMONA-III, No. 1/6, 35, 56," ScandPower (1980).

O. Øye, K. Haugset, and R. Holt, "RAMONA-III, A Program for Calculation of Transients in Boiling Water Reactors," ScandPower (1977).

3. IRT and RETRAN Modification and Evaluation

3.1 Once-Through Steam Generator Model - Mark II Version

The MARK II version of the once-through steam generator incorporated in IRT has run a TMI-2 type transient and the results are in good agreement with the results obtained using the MARK I version. Current work includes analyzing an overcooling transient for a typical B&W plant for comparison with the results obtained using the MARK I model. In addition, the IRT code is being modified such that the operation of two steam generators can be simulated independently.

3.2 Once-Through Steam Generator Analysis

Several letter reports have been issued describing the plant transient analysis of an overcooling transient for a typical B&W plant. These calculations have been performed using both the IRT and RELAP-3B codes.

3.3 IRT Code Modification

The programming that controls the main feedwater flow and auxiliary feedwater flow in the current IRT U-tube steam generator model has been adapted for use in both the MARK I and MARK II models. Currently, a routine that controls secondary side steam flow is being implemented into both models.

The implementation of the MARK I and MARK II once-through steam generator models with the steam flow and feedwater control systems in addition to the loop momentum equation (as described below) has caused the coding to exceed the limitations of the computer. Changes are currently being made in the loading sequence of the code to circumvent this problem.

3.4 IRT Loop Momentum Equation

The loop momentum equation is now operational in a separate version of the IRT code. The modelling includes the homologous pump model used in the RELAP codes. The momentum model is currently being implemented in the main version of the IRT code.

3.5 RETRAN Code Implementation and Modification

The version of the RETRAN code currently available at BNL has been modified to enhance the plotting capability on the BNL computer. Results produced by RETRAN can now be graphically superimposed with other data through the use of an auxiliary program.

4. TRAC ASSESSMENT AND MODEL DEVELOPMENT

4.1 Assessment of TRAC-P1A

4.1.1 University of Houston Flooding Tests (U. S. Rohatgi)

It was stated in the previous quarterly (Rohatgi, 1980) that the TRAC-P1A one-dimensional drift-flux formulation cannot simulate this countercurrent flow test due to an inadequate description of the relative velocity in the annular flow regime. Therefore, the two-fluid formulation of TRAC-P1A was investigated to see if it could predict the test. From a preliminary analysis of the Dukler and Smith (1977) experiment, it was found that the interfacial shear coefficient computed from the data in the flooded situation is four to five times greater than the Wallis correlation (1970) for the interfacial shear coefficient for annular flow.

Table 4.1 shows some of these computations for a case of 100 lb/hr liquid flow while the gas flow rate is increased. In this set of experiments flooding occurs around a gas flow rate of 250 lb/hr. This is evident in Table 4.1 from the sudden increase in the film thickness and the pressure gradient. The Wallis correlation is only good for the unflooded region of the countercurrent flow. Since TRAC-P1A uses the Wallis correlation for the interfacial shear in annular flow, it will underpredict the liquid carry-over with the incoming gas flow. This agrees with the conclusion reached by LASL personnel (Knight, 1980) when they simulated the Dartmouth College countercurrent flow test.

With this in mind, a literature search was undertaken to find a better correlation for the coefficient of interfacial shear. One such correlation developed by Bharathan (1979) was found, and it is being investigated. The expression is as follows:

$$f_i = 0.005 + A\,\delta^{*B}$$

where

$$\log_{10} A = -0.56 + 9.07/D^*$$

$$B = 1.63 + 4.74/D^*$$

$$\delta^* = \delta \Big/ \sqrt{\sigma/\left(g\left(\rho_f - \rho_g\right)\right)}$$

and

$$D^* = D \Big/ \sqrt{\sigma/\left(g\left(\rho_f - \rho_g\right)\right)}$$

Furthermore, f_i, δ, σ, ρ_f, and ρ_g are the interfacial shear coefficient, film thickness, surface tension, and liquid and vapor density, respectively.

TABLE 4.1

SHEAR COEFFICIENT IN COUNTERCURRENT
FLOW OF UNIVERSITY OF HOUSTON TESTS

W_ℓ lb./hr.	Wg lb./hr.	dp/dz cm of H_2O/cm	δ/D	α	$c_{fi,data}$	$c_{fi,Wallis}$	Remark
100	200	-0.004	0.0052	0.98	0.0122	0.0125	Not Flooded
100	240	-0.009	0.0052	0.98	0.02316	0.0125	Not Flooded
100	250	-0.037	0.009	0.96	0.08	0.0162	Flooded
100	260	-0.040	0.0086	0.97	0.086	0.0162	Flooded
100	270	-0.036	0.0062	0.975	0.072	0.0143	Flooded

4.1.2 Super-CANON Experiments (P. Saha)

The sensitivity of TRAC-P1A predictions to the initial water temperature has been studied for the Super-CANON test with a full-open discharge end and an initial water temperature of 280° C. In order to achieve a good prediction of the short-term pressure history, the initial water temperature for the TRAC calculation was taken as 270° C. This temperature is 10° C lower than the average initial test water temperature, and 8° C lower than the minimum temperature recorded by any thermocouple at the start of the transient. As shown in Figure 4.1, with this hypothetical initial water temperature of 270° C, TRAC-P1A predicts the short-term ($t < 0.1$ sec) pressure history quite well. However, the pressure thereafter is underpredicted, as in the original TRAC-P1A prediction.

The value of the void distribution parameter, C_o, was then changed from 1.1 (the original TRAC value) to 1.01 to reduce the relative velocity. The initial water temperature was still kept at 270° C, 10° C lower than the experimental value. The resultant TRAC prediction, also shown in Figure 4.1, was in close agreement with the data for the entire transient period. However, it must be kept in mind that two input changes, one of which is highly artificial, were needed to produce the good agreement. This confirms our previous observation that further examination of the TRAC-P1A models and the constraints (Rohatgi and Saha, 1980) placed on the code for the nonequilibrium phase change and relative velocity is required.

4.1.3 RPI Phase Separation Test (U. S. Rohatgi)

The simulation of the four high quality inlet flow tests--i.e., Tests 11, 14, 15, and 18, with TRAC-P1A has been completed, and the conclusions drawn in the previous quarterlies prevail. All four of the tests failed to converge to a steady-state. The code still produced an asymmetric solution for the two tests with symmetric boundary conditions and two outlets. These results are shown in Figures 4.2 and 4.3. As expected from the lower quality runs, the flow rates from the two outlets are further apart in Test 18 with rods than in Test 14 without rods. However, in the case of the other two tests with one outlet each (Tests 11 and 15) the code stopped due to overflow conditions. A topical report on the attempted assessment of TRAC-P1A with these tests is being written.

Some of the eight RPI tests that were attempted with TRAC-P1A without success will be tried again with the two-dimensional option of TRAC-PD2.

4.1.4 FRIGG-Loop Forced and Natural Circulation Test (L. Neymotin)

It was reported earlier (Neymotin, 1980) that the TRAC-P1A two-fluid model (1-D or 3-D) did not converge to a steady-state for the FRIGG rod bundle test because of numerical instabilities developed during the transient relaxation of the code. A number of 1-D vessel option runs directed at uncovering the major causes of the instabilities have been made during this quarter. Looking into the behavior of different field variables during the course of steady-state calculations with air-water and steam-water flows led to the belief that the problems could be in the area of interfacial heat and mass transfer

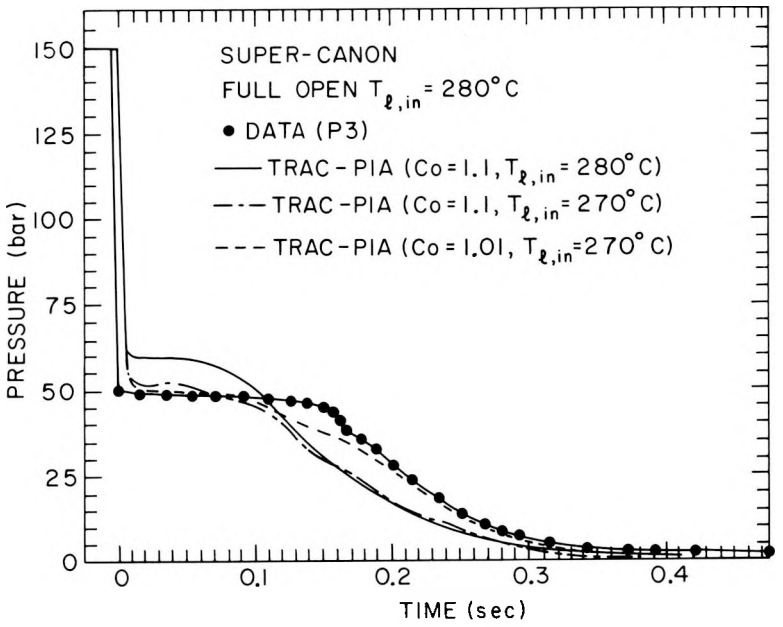

Figure 4.1. Effects of Initial Water Temperature and Void Distribution Parameter on the TRAC-P1A Prediction of a Super-CANON Test. BNL Neg. No. 10-50-80.

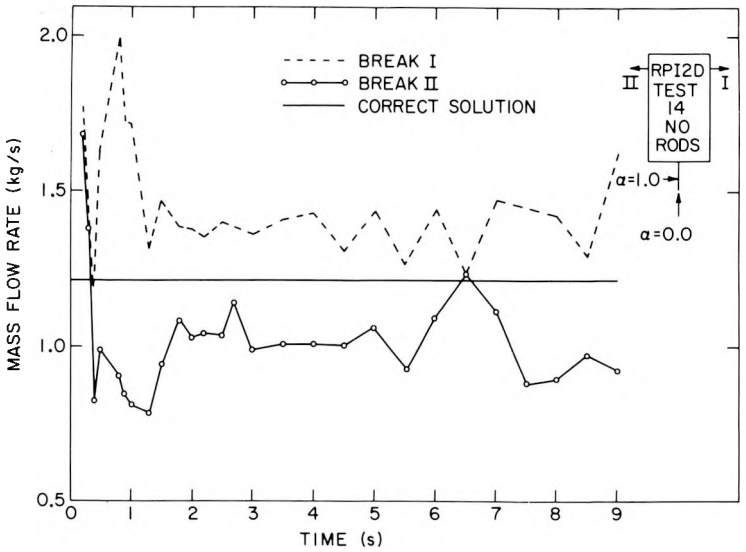

Figure 4.2. TRAC-P1A Calculations for RPI Test No. 14. BNL Neg. No. 10-393-80.

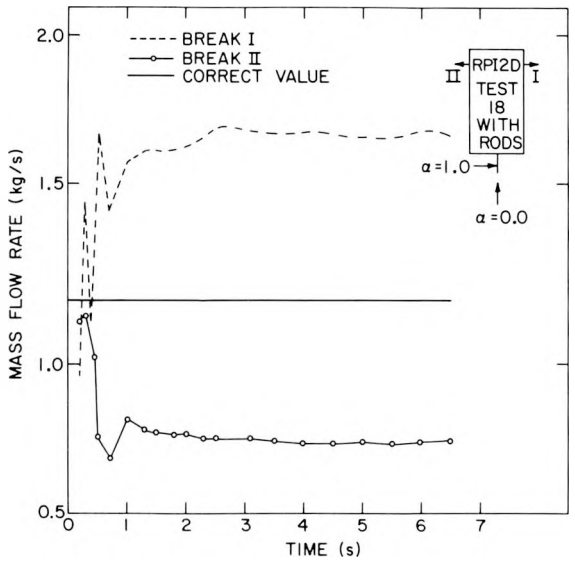

Figure 4.3. TRAC-P1A Calculations for RPI Test No. 18. BNL Neg. No. 10-394-80.

modeling. Specifically, the models selected for the bubbly and bubbly-slug flow regimes made the calculated interfacial heat flux (and, thus, the vapor generation rate) very sensitive to the relative velocity (see Equation 4.1). Thus a fluctuation in relative velocity makes the TRAC two-fluid numerical algorithm unstable.

To alleviate the problem, after a large number of time steps, say N_0, the relative velocity used in the vapor generation rate calculations has been replaced by an average value, $\bar{V}_r = \sum_{i = N_0}^{n} V_{r,i} \Big/ (n - N_0 + 1)$.

This modification resulted in a steady-state solution for a FRIGG rod bundle test using the one-dimensional two-fluid formulation of TRAC-P1A.

During the same period, a similar one-dimensional FRIGG calculation was performed with the TRAC-P1A drift-flux model--i.e., the PIPE component. Converged results were obtained with the drift-flux model without any modification. This may be due to the fact that in the bubbly and slug flow regimes the model uses correlations for relative velocity V_r, which depends mainly on the flow geometry, physical properties of the liquid, and void fraction (Equations 4.2 and 4.3). This might be considered as one of the principal differences between the two-fluid and drift-flux models that determine whether the particular model would be numerically stable.

A comment on the interfacial heat transfer should be made here based on the results obtained with the two formulations of TRAC. An interfacial heat transfer coefficient for a single bubble is used in both the bubbly and the slug regime for both the drift-flux and the two-fluid models. According to the code's logic, the larger of the two values for the heat transfer coefficients--i.e., sphere convection or the Plesset-Zwick model, is chosen. However, investigations revealed that $h_{i\ell,conv}$ (HLC) is always much larger than $h_{i\ell,Pl.-Z.}$ (HLC2), which makes the comparison just a formal action. Therefore, using the sphere convection model, the correlation for the interfacial heat flux per unit length can be written after some transformations in the form:

$$Q_{i\ell} \sim \frac{\alpha\,(T_s - T_\ell)\,V_r^{3.5}}{We^{1.5}} \qquad (4.1)$$

It appears from Equation (4.1) that the vapor generation rate, which is proportional to the interfacial heat flux, depends, among other items, on the relative velocity and the critical Weber number for bubbles.

For the drift-flux model in TRAC-P1A, the bubble Weber number has been assumed to be a constant and equal to 25, whereas V_r is supposed to be

calculated using the following correlations:

$$V_r = \begin{cases} \dfrac{1.41}{1-\alpha} \left[\dfrac{\sigma g (\rho_\ell - \rho_g)}{\rho_\ell^2}\right]^{1/4} & \text{(bubbly regime)} \quad (4.2) \\ \dfrac{0.345}{1-\alpha} \left[\dfrac{g D_h (\rho_\ell - \rho_g)}{\rho_\ell}\right]^{1/2} & \text{(slug regime)} \quad (4.3) \end{cases}$$

However, a logic implemented in the constitutive relations package prescribes a minimum value of 1.0 m/sec for the relative velocity when the void fractions vary from zero to 0.5. On the other hand, Equations (4.2) and (4.3) determine V_r to be equal to 0.18 to 0.36 m/sec in the same void fraction range. Because of the artificial restriction, a sharp rise in the interfacial heat transfer can be expected, as seen from Equation (4.1). Evidently this artificial increase in heat transfer and hence in vapor generation rate tends to reduce the "nonequilibriumness" of the model, and thus this model behaves very similarly to an equilibrium one.

Figure 4.4 shows the area averaged void fraction and $(T_\ell - T_s)$ vertical distributions in the bundle (the experimental void fraction curve starts earlier due to subcooled boiling which is not accounted for in TRAC-P1A). The dashed curve represents the void distribution which would have been obtained assuming that the flow were at equilibrium.

It is clear from these drift-flux model results that despite its nonequilibrium philosophy, TRAC behaves qualitatively and to a great extent quantitatively very similarly to an equilibrium code.

For the two-fluid formulation, the relative velocity is calculated explicitly as $(V_g - V_\ell)$ throughout the computation and is used in the interfacial heat transfer calculations. The critical Weber number for bubbles is assumed to be equal to 50. The impact of these model differences on the computed results is clearly seen in Figures 4.5 through 4.7, which display vertical distributions of some two-phase flow characteristics, as computed by the two-fluid as well as the drift-flux model of TRAC-P1A. The following features should be noted from those figures:

1. Void fraction for the two-fluid model increases along the rod-bundle more slowly due to the higher value of Weber number, We, and smaller values of the relative velocity and interfacial area (see Figures 4.5, 4.6).

2. Lowering the interfacial heat transfer in turn causes high nonequilibrium when a large amount of the heat is absorbed by liquid, thereby increasing the temperature differences $(T_\ell - T_s)$ considerably (see Figure 4.6)

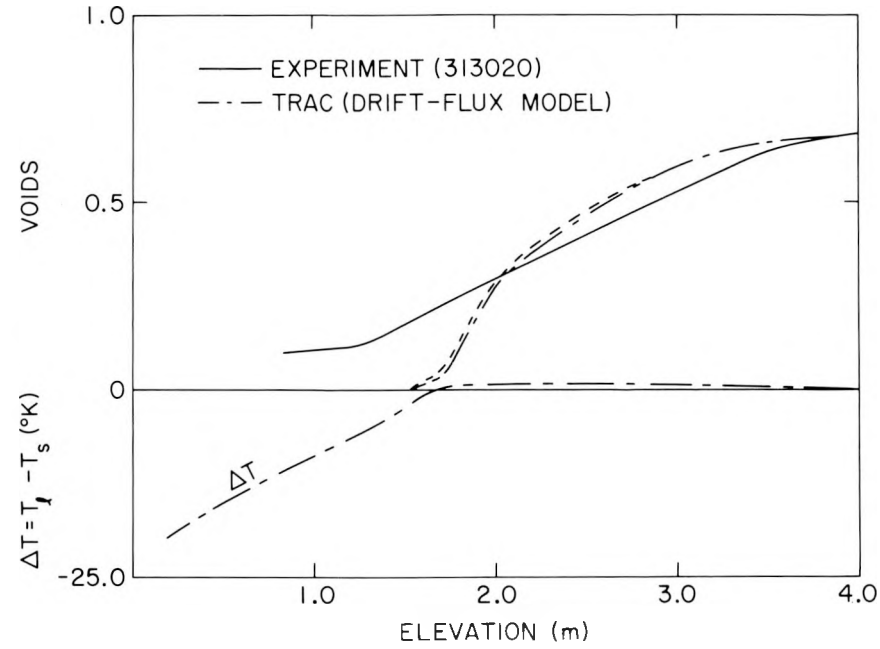

Figure 4.4. Void Fraction and (T_ℓ - T_s) Distributions in FRIGG's Rod-Bundle (Drift-Flux Model). BNL Neg. No. 10-53-80.

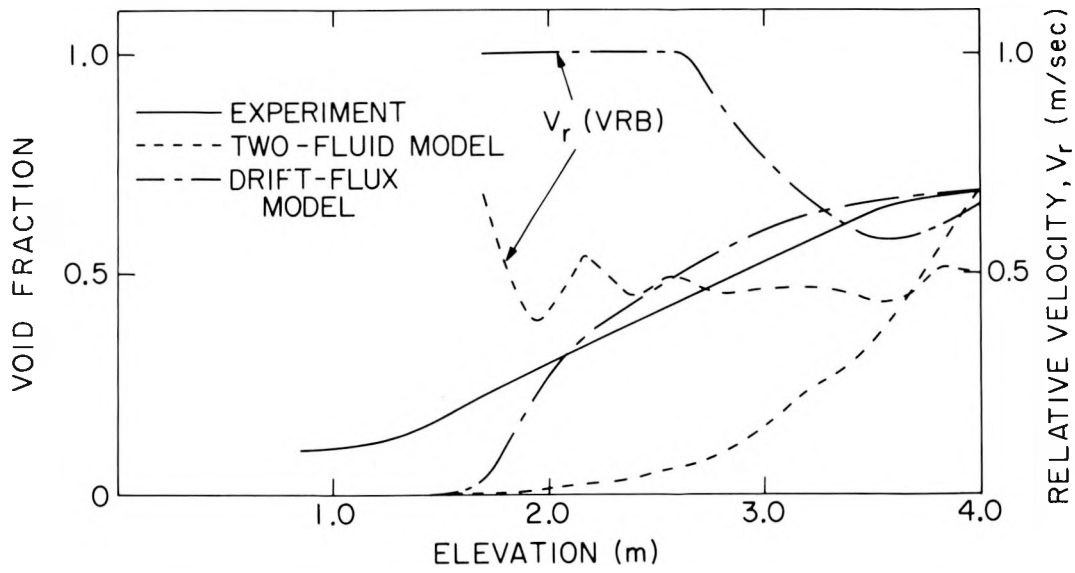

Figure 4.5. TRAC's Predictions of the Void Fraction and Relative Velocity for FRIGG Test (313020). BNL Neg. No. 10-49-80.

3. It can also be seen how abruptly the interfacial heat transfer increases and, as a result, the temperature difference (T_ℓ - T_s) drops when void fraction reaches the value of 0.5 (see Figures 4.5 through 4.7).

These results show that the two-fluid model of TRAC-P1A tends to underpredict the interfacial heat transfer which results in an unrealistically high nonequilibrium flow situation. A topical report on this activity is being prepared.

4.1.5 Assessment of Pump Model in TRAC-P1A (U. S. Rohatgi)

In the case of a small break LOCA or plant transients, the performance of the reactor coolant pumps can significantly affect the reactor core behavior. Any code which may be used to analyze these types of transients should have a good pump model; therefore, the TRAC-P1A pump model was examined. This model is the same as the one found in most codes such as RELAP4 and RELAP5. All of these models depend upon a degradation function which is assumed to be a function of void fraction only. However, it has been found from many experimental studies (Runstadler & Dolan, 1978, and Chen & Quapp, 1980) that the degradation is also a strong function of flow coefficient and specific speed. Furthermore, the TRAC-P1A pump model does not include the shaft work in the energy equations and the motor torque contribution in the angular momentum equation. All of these effects should be further investigated for the development of a better pump model.

4.2 Implementation of TRAC-PD2 (G. Slovik)

The TRAC-PD2 source program, Version 25.3, was received from LASL in July 1980 and was made operational on the BNL CDC-7600 machine. Seven of the sample problems supplied with the code were successfully executed, and results agreed with the LASL-supplied output within the minor difference of the two computer libraries. Running times at BNL were longer than at LASL; however, this was greatly reduced when the supplied COMPASS matrix inversion routines were made part of the BNL version. Efforts are still being made toward reducing the BNL running time since the BNL run times are still longer than LASL's, as seen from Table 4.2.

The associated plotting program (TRAP) supplied for TRAC-PD2 from LASL is being implemented at BNL.

4.3 Final Report on International Standard Problem 8 Calculations (P. Saha, U. S. Rohatgi, L. Neymotin, and G. Slovik)

The final documentation and analysis of all the calculations for the International Standard Problem 8--i.e., the Semiscale S-06-3 test (Collins, et al., 1978) began in the middle of August 1980. The calculations for the blowdown/refill stage of the transient can be grouped in the following categories:

(a) Calculations performed by using the RELAP4/MOD5 code; these were submitted by Italy and France.

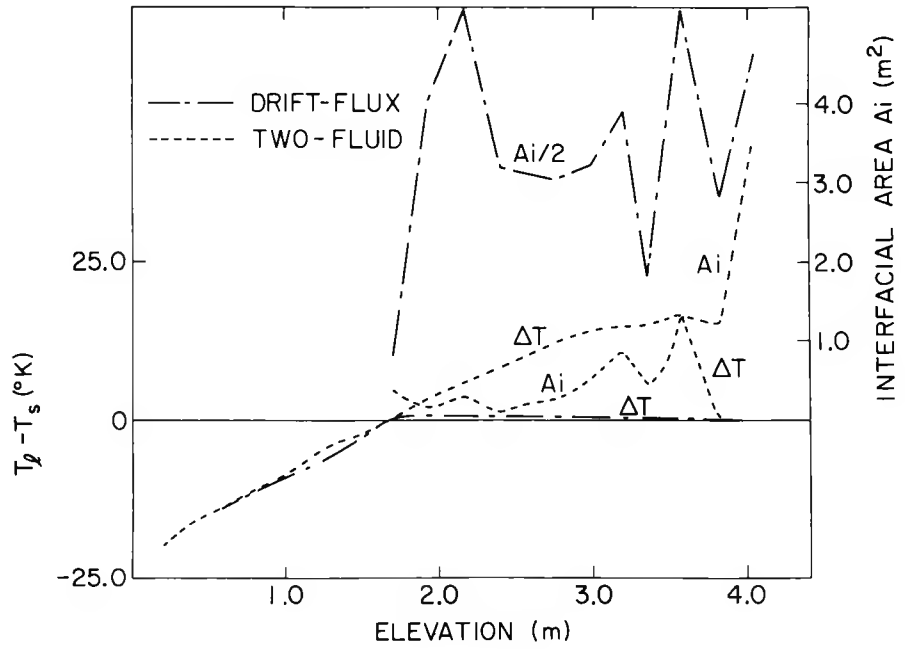

Figure 4.6. Calculated Interfacial Area and Temperature Differences vs. Vertical Distance. BNL Neg. No. 10-48-80.

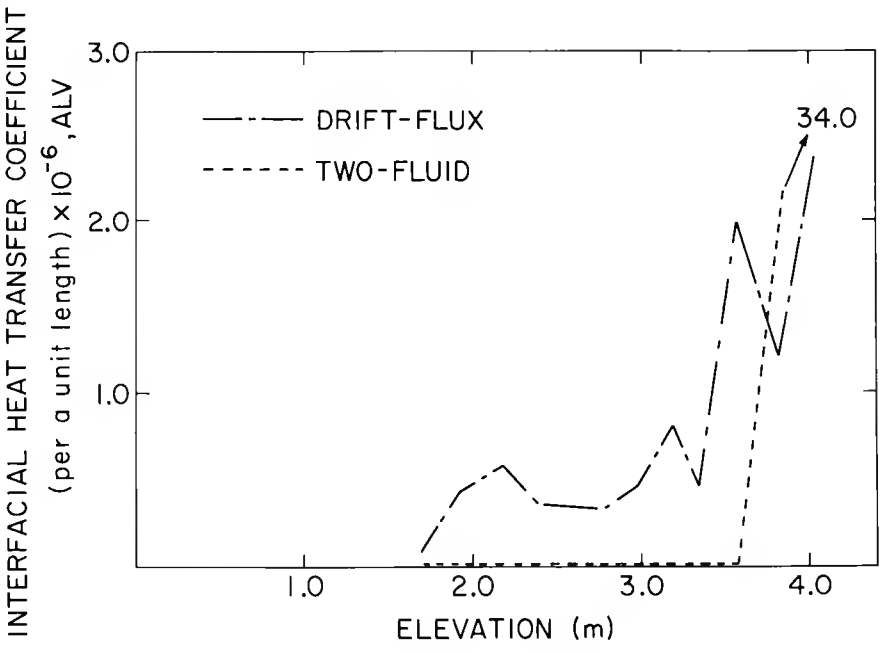

Figure 4.7. Comparison Between IHT Coefficients Obtained by Drift-Flux and Two-Fluid Models. BNL Neg. No. 10-51-80.

TABLE 4.2

A COMPARISON OF RUN TIME BETWEEN BNL AND LASL FOR TRAC-PD2

TEST	PROBLEM TIME (SEC)	CP TIME AT BNL (SEC)	CP TIME AT LASL (SEC)
Marviken III, (Test 4) One-Dimensional	15.02	53.52	45.37
FLECHT (Test No. 17201)	15.0	144.6	118.2
ECC Test from L2-2	10.0	102.2	71.43
TPRIZR (Pressurizer Test Problem	10.0	134.4	30.45
Marviken III, (Test 4) Three-Dimensional	5.016	162.7	149.7
Bennet Run 5336	15.00	174.7	145.2
CISE Heated Blowdown	0.5	158.7	129.3

(b) Calculations performed by using the RELAP4/MOD6 code; these were submitted by Finland, Sweden (two calculations, one in 1979 and the other in 1980), U.K., U.S.A. (INEL), National Power Company Limited (NPCL) of U.K., and Switzerland.

(c) Calculations performed by using other codes; these are calculations submitted by the Federal Republic of Germany by using the DRUFAN-01/MOD2 code, Japan by using the ALARM-P1 code, and U.K. by using the RELAP-UK Mark IV code.

Only four calculations for the reflood stage of the transient were submitted. All of them were performed by using the RELAP4/MOD6 code, and they were submitted by Finland, U.K., U.S.A. (INEL), and NPCL of U.K.

Recently INEL submitted a calculation performed by using the RELAP4/MOD7 code, and its results will also be included in the final report.

The report is being organized and written in such a way that the effects of user input can be examined by comparing the calculations obtained by using the same code--e.g., RELAP4/MOD6. In addition, emphasis is being placed on uncovering the possible reasons for the discrepancies between the various calculations and the experimental data.

At present the most time-consuming part of the work--i.e., preparation of the plots showing the comparisons of the various calculations with the experimental data, has been completed. It is expected that the first draft of the report will be completed in a month.

REFERENCES

BHARATHAN, D. (1979), "Air Water Counter Current Annular Flow," EPRI NP-1165, September 1979.

CHEN, T. H. and QUAPP. J. W. (1980), "Centrifugal Pump Performance Under Simulated Two Phase Flow Conditions," ASME Polyphase Flow and Transport Technology Symposium, August 1980.

COLLINS, B. L., et al. (1978), "Experimental Data Report for Semiscale Mod-1, Test S-06-3, LOFT Counterpart Test," NUREG/CR-0251, TREE-1123, July 1978.

DUKLER, A. E. and SMITH, L. (1977), "Two Phase Interactions in Counter Current Flow: Studies of the Flooding Mechanism," NUREG-CR-0617, Annual Report Nov. 1975 - Oct. 1977.

KNIGHT, T. D., et al. (1980), "TRAC-P1A Independent Assessment - 1979," 1980 Report.

NEYMOTIN, L. (1980), "FRIGG Loop Forced and Natural Circulation Tests," WRSRD Quarterly Progress Report," January - March 1980, BNL-NUREG-51218, June 1980.

ROHATGI, U. S. (1980), "University of Houston Counter Current Flow Tests," WRSRD Quarterly Progress Report, April - June 1980, BNL-NUREG-51255, September 1980.

ROHATGI, U. S., and SAHA, P. (1980), "Constitutive Relations in TRAC-P1A," NUREG/CR-1651, BNL-NUREG-51258, August 1980.

RUNSTADLER, P. W. and DOLAN, F. X. (1978), "Two Phase Flow, Pump Data for a Scale Model NSSS Pump, ASME Polyphase Flow in Turbomachinery Symposium, December 1978.

WALLIS, G. B. (1970), "Annular Two Phase Flow, Part 1: Simple Theory," Journal of Basic Engineering, Transaction of the ASME, pp. 59-72, March 1970.

II. METALLURGY AND MATERIALS EVALUATION

SUMMARY

The effects of service related variables on the stress corrosion cracking of Inconel 600 tubing are being determined experimentally and the data used to formulate a model for service life expectancy. Future tests will be conducted using full size U-bends and tubing to directly simulate active and passive denting which may occur in steam generators.

U-bend tests have established that coupling the Inconel 600 tubing to carbon steel promotes SCC more rapidly than any of the other environments investigated. Tests in progress indicate that crack initiation for several heats of Inconel 600 occurs 2 to 3 times faster in AVT than in pure water environments at 325°C.

Several tests have been completed to determine the crack initiation time of tube type specimens tested using a constant extension rate. The crack initiation time for materials without any cold work are longer than those that have been rolled into plate. This will make the effect of cold work on the crack velocity less than the factor of two previously reported.

Constant load tests have been conducted to establish the stress dependency on crack initiation in pure water at 345°C.

1. Stress Corrosion Cracking of PWR Steam Generator Tubing

(T.S. Bulischeck and D. van Rooyen)

A model for predicting the remaining useful servie life of steam generator tubing is being developed using quantitative data obtained from laboratory investigations of the variable which may influence the stress corrosion cracking of Inconel 600 tubing. The effects of metallurgical structure, temperature environment stress or strain level and strain rate are being investigated. Phase I of this project developed quantitative data on these variables and it was agreed during recent discussions with Dr. P. Wu, RSR Program Manager, that Phase 2 of this project will be conducted using specimens which directly simulate the denting action on full size tubes and small radius U-bends in the steam generator. The data developed during this quarter using tests to determine stress corrosion cracking incubation times or propagation rates are as follows:

1.1 Constant Deflection Tests

Reverse tube U-bend specimens are being used to provide crack initiation times for statically stressed specimens. The strains in these specimens approach 40% near the apex of the bend. Localized dent specimens with dents of 5, 20 or 40 mils are also being tested to establish a relationship between dent depth and initiation time. Constant deflection tests that have been completed or are currently in progress are listed along with the failure times of the various materials in Table 1. Heats #2, 3, 4, 5, 10, 11 and 13 are mill annealed materials with microstructures showing little evidence of chromium carbide precipitates. Heats #17, 18 & 20 are currently manufactured tubing removed from the mill prior to the final thermal treatment at 700°C for 15 hours. These materials have a sensitized structure. Heats #14, 15, 16 & 19 are tubing which has been given a final heat treatment at 700°C for 15 hours to produce a semi-continuous chromium carbide precipitate without a chromium depleted zone. Only six of these 14 did not fail, two of these were mill annealed and the remaining four were all of the thermally treated materials.

Figure 1 compares the effect of recently completed tests containing carbon steel, which was used to construct dent specimens, and other test conditions, i.e. pickling or primary water. Coupling the Inconel 600 to carbon steel shifts the potential cathodic relative to the open circuit potential and produced SCC in all of these susceptible heats in approximately the same exposure time. This results in an acceleration of the failure time by a factor of 8 in the worst case.

Several failures have occurred during this reporting period in AVT environments at 325°C. Figures 2 and 3 show that the data for the AVT environments parallel the results of the pure water exposures and indicate that the

activation energy for crack initiation is not changed by the different environments. AVT environments initiate SCC 2.5 to 3 times faster than pure water environments for these heats of material.

1.2 Constant Extension Rate Tests

The constant extension rate test is used to determine crack propagation rates for the material investigated in this program. Previously reported results showed that while the incubation period for SCC is minimized using this test method, that time must be established in order to accurately calculate the crack propagation rates. This data has been reported for specimens which were flattened into plate and tested with some cold work as a result of the rolling. Several tests have been completed during this quarter to establish the initiation time of dual ligament type tensile specimens that do not have any additional cold work. Figure 4 indicates that the initiation for the material without cold work is longer, however, several additional tests will be conducted to establish the initiation time before the crack velocities for tube specimens can be corrected. The data at this time suggests that the crack velocities for the tube and plate type specimens will not be as different as a factor of 2 which was previously reported.

1.3 Constant Stress Tests

Constant load tests used to define the effect of stress on crack initiation times of 365°C indicate that the failure time is inversely proportional to σ^3, however, there is some scatter in this data. The effect of stress on initiation time at 345°C has been determined at one stress level and the results are shown in Fig. 5. Additional tests are necessary to determine whether the same stress to failure time relationship exists at this temperature.

TABLE 1

CRACK INITIATION TIME OF CONSTANT DEFLECTION SPECIMENS

Heat No.	Pure Deaerated H_2O 365°C 36 Wks	Pure Deaerated H_2O 345°C 36 Wks	Pure Deaerated H_2O 325°C 82 Wks*	Pure Deaerated H_2O 290°C 111 Wks	H_2O + Carbon Steel 365°C 9 Wks*	Primary H_2O 365°C 23 Wks	Primary H_2O 345°C 10 Wks	AVT 345°C 24 Wks	AVT 325°C 26 Wks*
2	2 2P	14 16P	NC	NC	2	4	8	5	20
3	NC	NC	NC	NC	NT	NC	NT	NC	NT
4	11	10P	51	NC	1.5	12	5 3P	7	20 16P
5	13 9P	16 13P	29P	NC	3	NC	9P	19	NC
10	2P	5P	NC	NC	2P	22 1P	3P	8P	NC
11	13 4P	16P	NC	NC	3	22 1P	6P	11P	NC
13	NC	NC	NC	NC	NT	NC	NT	NT	NT
14	NT	NT	NT	NT	NC	NC	NC	NC	NC
15	NT	NT	NT	NT	NC	NC	NC	NC	NC
16	NT	NT	NT	NT	NC	NC	NC	NC	NC
17	NT	NT	NT	NT	4P	14P	NC	17P	NC
18	NT	NT	NT	NT	4P	17P	3P	9P	NC
19	NT	NT	NT	NT	NC	NC	NC	NC	NC
20	NT	NT	NT	NT	3P	5P	NC	NC	NC

* Test Continuing
P = Pickled Specimens
N.C. = No Cracking
N.T. = Not Tested